Utrecht University

Coupled free-flow and porous media flow: a numerical and experimental investigation

Master's Thesis

Pavan Cornelissen
3863514

Supervisors:
Kilian Weishaupt, MSc
prof. dr. ir. Rainer Helmig
prof. dr. ir. Majid Hassanizadeh

Environmental Hydrogeology Group
Department of Earth Sciences
Faculty of Geosciences
Utrecht University

Contents

List of Figures

List of Tables

Abstract

Modelling situations containing a freeflow region and adjacent porous medium is challenging due to the different model concepts in both domains. The interface can be described as either a sharp surface or a thin layer with complex properties using a pore-network model. In this study, the first step is taken by coupling a freeflow model with a pore-network model. Additionally, the interface is investigated experimentally using confocal microscopy. The velocity field is determined using particle tracking. Both single-phase and two-phase flow have been considered in the pore-network model. In the case of two-phase flow, the freeflow domain is occupied by the non-wetting phase.
The single-phase model is able to recreate the flow patterns found in the experiments. However, the exact setup could not be recreated in the model, because of the large pore sizes of the micromodel. This leads to large flow velocities at the interface and creates problems for the Stokes model. The two-phase is not able to simulate the conditions of the experiments, because in the experiments, flow of water occurs without invasion of the pore-network by the non-wetting phase. For future work, the pore-network is to be coupled to a macroscopic porous medium model. For this purpose, additional boundary conditions have to be defined for the two-phase pore-network model. Furthermore, the model can be extended to include heat and component transport.

Keywords: coupled freeflow-porous media flow, Stokes equation, Beavers-Joseph condition, pore-network modeling, multiphase flow.

1 Introduction

Interactions between free fluid flow and porous media flow occur in numerous problems of interest. There are applications in the environmental, medical and industrial field. For example, wind-driven evaporation of soil water, drug-transport in the human body from the blood vessels to surrounding tissue and flow in fuel cells (e.g. Discacciati and Quarteroni (2009), Ehrhardt (2010), Jambhekar et al. (2015)). The interactions between the two domains is determined by the processes that occur at the interface between the two domains. For simulations of the aforementioned applications, these processes must be investigated. This works aims at doing so by both numerical and experimental investigations.

There are two main methods of solving the fluid flow in coupled free flow and porous media flow. One method is to split the domain in two separate regions: one region for the free flow and one for the porous medium. The Darcy equation is solved in the porous medium and the Navier-Stokes equation is solved in the free flow region (Figure 1b). At the interface where the two domains meet, an interface layer is present. In order to couple the two domains, appropriate boundary conditions must be chosen at the interface between porous medium and free flow. This proves to be challenging, as the Navier-Stokes and Darcy equations are of a different order (Das and Lewis, 2007).

Another method is the single domain approach (Figure 1a). In this case, the Brinkman equation is used, which is an extended form of Darcy's law with an extra inertial term (Brinkman, 1947). This equation is solved in the entire domain, but different spatial parameters, like porosity and permeability, are used in the free flow region and porous medium. Instead of a sharp interface, a transition zone is present where the spatial parameters show a continuous transition between the values in the free flow domain and the porous medium. No coupling conditions have to be assigned at the interface as continuity of stresses and velocity is already achieved. However, it is very difficult to determine the appropriate parameter values in the transition zone, and the choice of parameter values has a large influence on the results (Goyeau et al., 2003).

Therefore, the two-domain approach is often preferred. The processes between the free-flow and porous medium regions are not only interface-driven, but a transition zone is present where changes in fluid properties and gradients in driving forces occur (Mosthaf et al., 2011). According to (Hassanizadeh and Gray, 1989), the interface between the porous medium and the adjacent free flow region can be approximated as either a simple or a complex interface. A simple interface has no thickness and is not able to store mass, momentum or energy.

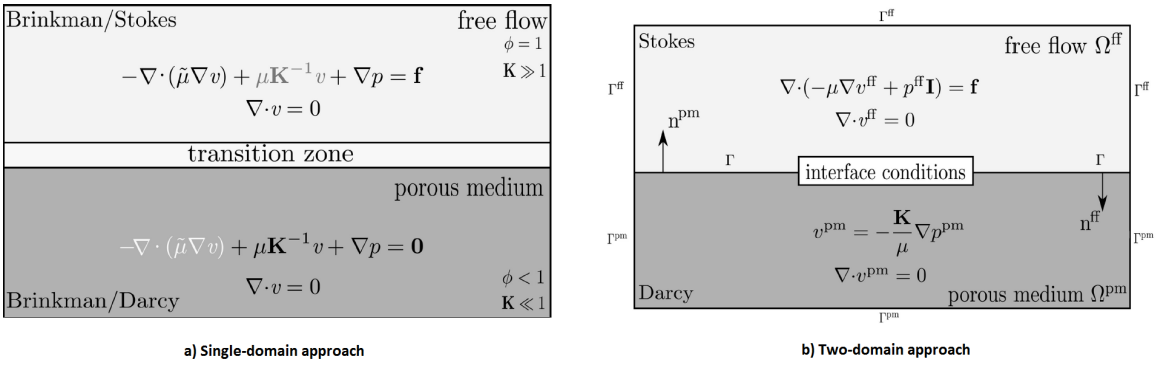

Figure 1: Coupling concepts for a single-domain approach and a two-domain approach (Mosthaf et al., 2011)

Thermodynamic equilibrium is often assumed for coupling conditions. However, the concept of a simple interface might not be able to describe all the processes occurring at the interface between the free flow domain and porous medium. The processes between the two domains is strongly dependent on the properties of the interface layer. Thus, a complex interface is required. A complex interface has a thickness, although it is very small compared to the two adjacent domains and storage of thermodynamic quantities is possible. In order to obtain a meaningful coupled model, the complex processes in the interface layers must be adequately described. A possible method of describing the interface layer between the free flow region and the macroscale porous medium region involves using a pore-network model between the two flow regimes (Baber, 2014). A schematic representation of the concept is shown in Figure 2. Pore-network models are used to model flow and transport in porous

media at the microscale. Macroscopic parameters can be obtained by averaging the pore-scale results over a representative volume.

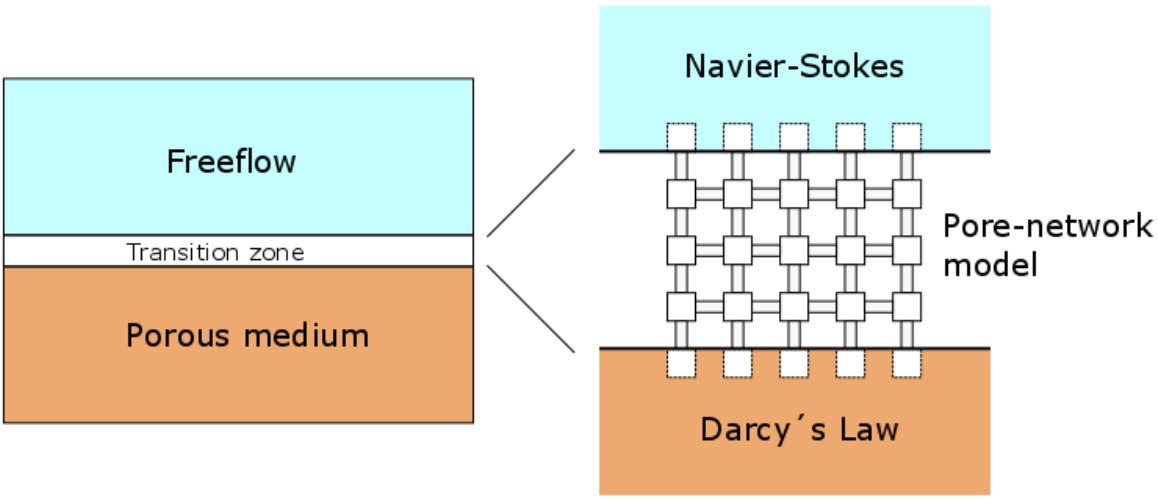

Figure 2: A free flow region and a porous medium coupled by an interface layer represented as a pore-network model.

In this study, only the first step of coupling the free flow region and porous medium by means of a pore-network model will be realized. This step consists of coupling the free flow region to a pore-network model. First, this will be done for single-phase flow within both the free flow region and the pore-network model. Then, the model will be extended to single-phase free flow and two-phase flow in the pore-network model. The non-wetting phase will be present in the free flow region. The flow in both regions is considered to be isothermal and non-compositional. Therefore, only momentum and mass transfer across the interface is investigated. Additionally, the interface between porous medium and free flow will be investigated experimentally using confocal microscopy. Using particle tracking, the flow velocities in the porous medium can be obtained. Thus, flow in the porous medium induced by the momentum transfer along the interface is investigated and will be compared to the results of the numerical study.

The report is structured as follows:

- A literature review is given in Chapter 2.
- The models and the experimental setup is discussed in Chapter 3.
- The results of the simulations and the experiments are presented and discussed in Chapter 4.
- The work is summarized in Chapter 5.

2 Background

Before describing the equations used in the models, the fundamentals of freeflow and pore-network modelling will be given in this section. First, relevant fluid properties will be discussed. Then, a general overview of pore-network models is given. Finally, coupling concepts used in previous studies will be reviewed.

2.1 Fluid properties

2.1.1 Fluid stresses

Fluid particles in motion are affected by two types of forces: surface forces or stresses and body forces. The only body force relevant in this case is gravity. Stresses develop because of the interaction between fluid particles which move with different flow velocities. The magnitude of the forces depends on the viscosity of the fluid. The stress tensor σ is given by:

$$\bar{\bar{\sigma}} = \begin{pmatrix} \sigma_{xx} & \tau_{xy} & \tau_{xz} \\ \tau_{yx} & \sigma_{yy} & \tau_{yz} \\ \tau_{zx} & \tau_{zy} & \sigma_{zz} \end{pmatrix} \tag{1}$$

where σ and τ are the normal and tangential components of the viscous stress, respectively. The stress tensor can be separated into two terms: the pressure term and the deviatoric stress tensor. The pressure only acts on the face normal and is therefore multiplied by the identity tensor.

$$\bar{\bar{\sigma}} = \bar{\bar{\tau}} - p\bar{\bar{I}} \tag{2}$$

where τ is the deviatoric stress tensor:

$$\bar{\bar{\tau}} = \begin{pmatrix} \sigma_{xx} + p & \tau_{xy} & \tau_{xz} \\ \tau_{yx} & \sigma_{yy} + p & \tau_{yz} \\ \tau_{zx} & \tau_{zy} & \sigma_{zz} + p \end{pmatrix} \tag{3}$$

2.1.2 Newton's law of viscosity

The stresses in a fluid occur due to the fact that layers of fluid particles move at different velocities. This creates a shear stress, which magnitude depends on the magnitude of the velocity gradient. If the shear stress is linearly related to the velocity gradient, the fluid is considered to be a Newtonian fluid. The proportionality constant is the dynamic viscosity μ.

$$\tau_{ij} = \mu\left(\frac{\partial v_i}{\partial x_j} + \frac{\partial v_j}{\partial x_i}\right) \tag{4}$$

Thus, the deviatoric stress tensor in Equation 3 can be rewritten as:

$$\bar{\bar{\tau}} = \mu \begin{pmatrix} 2\frac{\partial v_x}{\partial x} & \frac{\partial v_x}{\partial y} + \frac{\partial v_y}{\partial x} & \frac{\partial v_x}{\partial z} + \frac{\partial v_z}{\partial x} \\ \frac{\partial v_y}{\partial x} + \frac{\partial v_x}{\partial y} & 2\frac{\partial v_y}{\partial y} & \frac{\partial v_y}{\partial z} + \frac{\partial v_z}{\partial y} \\ \frac{\partial v_z}{\partial x} + \frac{\partial v_x}{\partial z} & \frac{\partial v_z}{\partial y} + \frac{\partial v_y}{\partial z} & 2\frac{\partial v_z}{\partial z} \end{pmatrix} \tag{5}$$

2.1.3 The Navier-Stokes equation

Newton's second law states that the sum of the forces acting on a particle equals the mass times acceleration of said particle.

$$\Sigma F = ma \tag{6}$$

For a constant control volume, the mass can be replaced with density. The acceleration can be written as the total derivative of the velocity. The forces acting on the fluid are the stresses and gravity. Using the separation of the stresses into two terms as shown in Equation 2, the following expression is obtained for the momentum balance, which equals the Navier-Stokes equation:

$$\rho(\frac{\partial \bar{v}}{\partial t} + \bar{v} \cdot \nabla \bar{v}) = -\nabla p + \nabla \cdot \bar{\bar{\tau}} + \rho \bar{g} \tag{7}$$

The first term describes the change of momentum in time, the second term describes the inertial forces, the third term describes the pressure forces, the fourth term describes the viscous forces and the final term describes gravity forces.

2.1.4 Reynolds number

The Reynolds number describes the ratio of the inertial and viscous forces in a fluid. The Reynolds number is defined as:

$$Re = \frac{\rho v L}{\mu} \tag{8}$$

where ρ is the fluid density, v is the fluid flow velocity, μ is the dynamic viscosity of the fluid and L is a characteristic length. In a capillary channel, the characteristic length is often taken as the diameter of the tube, while in porous media it is taken as the median grain size or pore size. When the inertial forces are small, the Reynolds number is small. Laminar flow occurs in this regime and inertial forces can be neglected in this case. The inertial forces are dominant for large Reynolds numbers and turbulent flow occurs. The threshold values for the different flow regimes also differs per application. For flow in pipes, laminar flow occurs when the Reynolds number is smaller than 2300 and turbulent flow occurs when the Reynolds number is larger than 3500. For Reynolds numbers between these two values, a transition regime occurs. In porous media, the Reynolds number should be smaller than 1 for laminar flow to occur. For laminar free flow, the inertial term in the Navier-Stokes equation can be neglected to obtain the Stokes equation:

$$\rho \frac{\partial \bar{v}}{\partial t} = -\nabla p + \nabla \cdot \bar{\bar{\tau}} + \rho \bar{g} \tag{9}$$

2.2 Pore-network models

A pore-network model is a simplified representation of a porous medium. The pore space is discretized in nodes and connections; referred to as pore bodies and pore throats, respectively. The pore bodies represent the larger open spaces within the pore-network, while the pore throat represent the narrow connections between these pore bodies. The pore elements often have simple shapes, like cubes, spheres or cylinders. Flow between the pores is calculated using a simplified form of the Navier-Stokes equation, like the Hagen-Poiseuille equation. Flow and transport equations are written for the pore-scale. By averaging the results over the network, macroscopic flow parameters can be estimated. Pore-network models can also be used for multiphase flow. For example, capillary pressure-saturation relationships can be estimated. For these cases, square or triangular cross-sections are used for the pores, so that the wetting phase can occupy the corners of the pores, while the non-wetting phase occupies the center of the pores (Figure 3). These descriptions of the pore geometry allow for better agreements with experiments (Blunt, 2001).

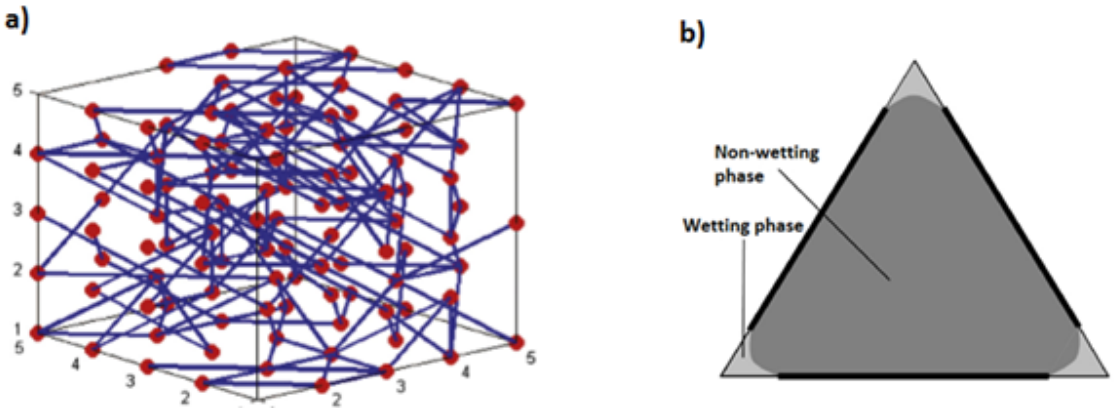

Figure 3: a) Example of a pore-network model. The nodes are pore bodies, the connections are the pore throats (Raoof et al., 2013). b) Phase distribution in angular pore throats. The corners are occupied by the wetting phase, while centers are occupied by the non-wetting phase (Blunt, 2001).

Quasi-static pore-network models are often used for calculating the relative permeability of a porous medium. However, quasi-static models are only valid for equilibrium conditions. The equilibrium distribution between the wetting-phase and non-wetting phase is used for the calculation of fluid flow through the pore-network. Thus, the assumption is made that enough time has passed in order to reach this equilibrium state. The amount of time required can be up to days or weeks. However, the fluid movement at the start can be very rapid. Also, the model gives no information about the time required in order to reach this state. Quasi-static pore-network models are therefore not able to capture the transient effects in a multi-phase system. This is why dynamic pore-network models have been created, which are able to model the dynamic properties. These models give more realistic values for the relative permeability. However, these models are computationally more expensive.

2.3 Coupling concepts

At the interface between porous medium and free-flow domain, appropriate boundary conditions must be applied to obtain an meaningful coupling. Thermodynamic equilibrium is assumed, although it is not always possible to achieve. Due to different model concepts, jumps in thermodynamic properties can occur.

2.3.1 Normal stress and mass flux

Continuity of mass flux and normal stress is often used as a coupling condition at the interface between porous medium and free-flow domain (e.g. Layton et al. (2003)). Alternatively, a jump in the normal stress is used in Ochoa-Tapia and Whitaker (1995). To the author's knowledge, no publications have been about coupled free flow regions and pore-network models. However, a similar approach is used in Baber (2014). A bundle-of-tubes is used to derive macroscale coupling conditions. The freeflow region and the porous medium are connected by a thin layer containing numerous cylindrical tubes. The tubes go straight from the freeflow domain to the porous medium and are not connected with each other. At the interface, the coupling conditions that are chosen are continuity of mass flux and continuity of normal stress. Since fluids in the pore-network model are assumed to be incompressible, the mass flux from the free flow region into the pore-network must be equal to the outflow of the pore-network model. For conservation of mass, the following condition is used for single-phase flow:

$$\left[\rho_g \bar{v_g} \cdot n\right]^{pm} = \left[\rho_g \bar{v_g} \cdot n\right]^{ff} \tag{10}$$

where the superscript pm stands for the porous medium, and ff for the free flow region. Since the pressure in the pore-network model is not averaged, unlike in a macroscopic porous medium, the pressure in the freeflow domain is equal to the pressure in the pore-network. Mechanical equilibrium is obtained by equilibrium of normal stresses. In the pore-network model, only the pressure forces are taken into account. In the free-flow model, the normal shear stresses are added to this. For single-phase flow, this is obtained by (Baber, 2014):

$$\left[n \cdot ((p_g I - \tau)n)\right]^{ff} = p_g^{top} \tag{11}$$

In the case of two-phase flow, the capillary pressure also plays a role. Differentiation must be made between water-filled and gas-filled pores. Following Baber (2014), an area-weighted average is used to obtain the following expression for mechanical equilibrium water as non-wetting phase (hydrophobic medium):

$$\left[n \cdot ((p_g I - \tau)n)\right]^{ff} A_\Gamma = p_g^{top} A_g + (p_w^{top} - p_c) A_l \tag{12}$$

where A_g is the area of gas-filled pores and A_l the area of liquid-filled pores. However, in the work of Baber (2014), it is assumed that a pore is completely filled with either the water or gas phase. This is not the case for a pore-network model, which is capable of handling two phases being present in a single pore. Equation 11 shows that a pressure discontinuity occurs at the interface, which occurs due to different concepts of the two models. The existence of a discontinuity in pressure is not realistic, as pressure is usually a continuous property at the microscale (Mosthaf et al., 2011). The pressure discontinuity is a consequence of choosing continuity of normal stress as a coupling condition. When continuity of pressure is chosen as the coupling condition, the normal stress will be discontinuous at the interface. Coupling conditions for the pore-network model will be similar to the bundle of tubes concept, but the actual coupling conditions will be derived in Chapter 3.

2.3.2 Tangential velocity at the interface between porous medium and free flow domain

For Newtonian fluid flow over a porous structure, a boundary condition for the tangential component of the velocity is required for the free flow domain at the interface. The velocity changes rapidly from its value in the freeflow domain to its value in the porous medium. This rapid transition can be approximated by a jump in the tangential velocity, given by the Beavers-Joseph equation. The slip-velocity at the interface in the freeflow domain is related to the velocity difference between the two domains and the velocity gradient inside the free flow region (Beavers and Joseph, 1967). For a two-dimensional problem, this can be written as:

$$\frac{\partial v_x}{\partial y} = \frac{\alpha_{BJ}}{\sqrt{\kappa}} \left(v_x^{ff} - v_x^{pm} \right) \tag{13}$$

Here, α_{BJ} is the Beavers-Joseph coefficient, κ is the intrinsic permeability of the porous medium, v_x^{ff} is the velocity in the freeflow domain at the boundary and v_x^{pm} is the velocity inside the porous medium. The value of α_{BJ} is dependent on the structure of the grains at the interface and must be determined experimentally.

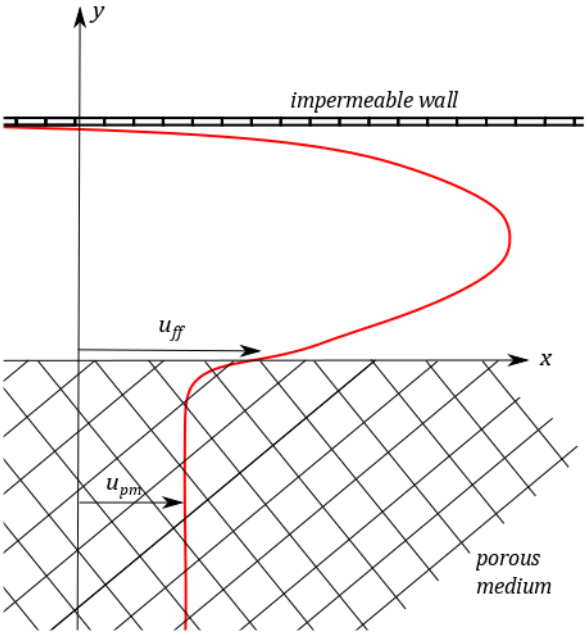

Figure 4: Slip velocity inside porous medium. The red line shows the tangential flow velocity. It equals zero at the impermeable wall at the top and approaches the tangential velocity in the porous medium (Beavers and Joseph, 1967).

The Beavers-Joseph condition has also been derived by volume averaging by Saffman (1971). Neglecting the tangential velocity in the porous medium the Beavers-Joseph-Saffman can be written as ((Layton et al., 2003)):

$$\left[\left(v - \frac{\sqrt{K_i}}{\mu \alpha_{BJ}} \tau \cdot n \right) \cdot t_i \right]^{ff} = 0 \tag{14}$$

It should be noted that the Beavers-Joseph relation is derived for a case where there is parallel flow in the porous medium and free flow domain. Thus, in the case of Figure 4, the flow must be in x-direction. The simulations in this study investigate mainly pressure differences in the y-direction. The Beavers-Joseph relation is derived for single-phase flow. However, in this study it will also be applied to a multi-phase problem. The application of the Beavers-Joseph coefficient is therefore questionable. However, the importance of the tangential velocity at the interface in the free flow domain is to be determined.

3 Methods

In the previous section, the fundamental concepts and processes have been described. Now, the models and the experimental setup will be described in greater detail. This study contains both a numeric and an experimental investigation of the interface between freeflow and porous medium. First, the freeflow and the pore-network model will be described. Secondly, the coupling conditions at the interface will be derived and presented. Thirdly, the values of the parameters and boundary conditions used in the model will be given. Finally, the experimental setup will be discussed.

3.1 Simulations

3.1.1 Free-flow model

Laminar flow will be considered in this study. Thus, flow velocities must be small to ensure the Reynolds number is less than 2300. The inertial term can be neglected and thus the Stokes equation is solved. The equation is solved in the open-source simulator Dumux (Flemisch et al. (2011), Schwenck et al. (2015)). The Stokes equation is given by:

$$\rho \frac{\partial \bar{v}}{\partial t} = -\nabla p + \nabla \cdot \bar{\bar{\tau}} + \rho \bar{g} \tag{15}$$

It is solved together with the mass balance equation for the fluid:

$$\frac{\partial \rho}{\partial t} + \nabla \cdot (\rho \bar{v}) = 0 \tag{16}$$

3.1.2 Pore-network model

3.1.2.1 Single-phase pore-network model

The followings assumptions are made:

- Since pore throats are the narrowest elements in the pore-network, the conductivity of the pore throats determines the permeability of the pore-network. The resistance to flow in pore bodies is assumed to be negligible.
- The fluids are incompressible and the solid matrix is not deformable.
- Fluid flow in pore throats is assumed to occur at low Reynolds number conditions. This validates the use of the Washburn equation for fluid fluxes.
- Flow is only induced by an applied pressure difference across the boundaries. Gravity effects are not included in the model.

Because the fluid is incompressible, the sum of the fluxes within a pore body must be equal to zero:

$$\sum Q_{ij} = 0 \tag{17}$$

The flux in a pore throat is given by the following equation (Acharya et al., 2004):

$$Q_{ij} = K_{ij}(P_i - P_j) \tag{18}$$

where Q_{ij} is the volumetric flow rate in the pore throat connecting pore i and j, K_{ij} is the conductivity of the pore throat, P_i and P_j are the pressure in pore i and j, respectively. The conductivity of a pore throat is defined as:

$$K_{ij} = \frac{\pi}{8\mu l_{ij}} (r_{ij}^{eff})^4 \tag{19}$$

Here, μ is the dynamic viscosity of the fluid, l_{ij} is the length of the pore throat and r_{ij}^{eff} is the effective pore throat radius, which, for a square cross-sectional throat, is defined as:

$$r_{ij}^{eff} = \sqrt{\frac{4}{\pi}} r_{ij} \tag{20}$$

Substituting Equation 18, Equation 19 and Equation 20 into Equation 17, a set of i linear equations with i unknowns is obtained, which can be solved numerically to obtain the pressure in each pore body.

3.1.2.2 Two-phase pore-network model

The pore-network model used is based on the model described in Joekar-Niasar (2010), although the computational procedures are different. In addition to the assumptions stated in section 3.1.2.1, the following assumptions are added for two-phase flow conditions:

- The fluids are immiscible.
- The volume of pore throats is negligibly small compared to the volume of pore bodies. Therefore, the time required to fill pore throats is negligible compared to the time to fill pore bodies. Also, the volume of pore throats is not included when calculating the network saturation.

When two phases are present in porous media, the wetting phase will occupy the corners of the pore space. Flow along the sides of the pores is called corner flow, and can be a significant contribution to the relative permeability. In order to include this process, cubic pore bodies are used in the model. The model uses a two-pressure algorithm. This means that when a pore body is filled with two fluids, each fluid has its own pressure (e.g. Thompson (2002)). The local capillary pressure for pore body i is defined as the difference between the local non-wetting pressure and the local wetting pressure:

$$p_i^c = p_i^n - p_i^w = f(s_i^w) \tag{21}$$

Since the fluids are assumed to be incompressible, the following volume balance holds for a single pore:

$$\sum Q_i^n + \sum Q_i^w = 0 \tag{22}$$

Here, Q_i^n and Q_i^w are the non-wetting phase flux and wetting-phase flux through pore i, respectively. Using the Washburn formula (Washburn, 1921), the fluid flux through a pore can be described by the product of a pore throat conductivity and the pressure difference between the pores. Thus, Equation 22 can be written as:

$$\sum Q_i^\alpha = \sum K_{ij}^\alpha (P_i^\alpha - P_j^\alpha) \tag{23}$$

Here, for a certain phase α, K_{ij}^α is the conductivity for the pore throat connecting pore body i and j. The pore throat conductivity is a function of the throat geometry and fluid saturation. An additional volume balance for each phase is used to calculate the saturation change:

$$V_i \frac{\Delta S_i^\alpha}{\Delta t} = -\sum Q_{ij}^\alpha \tag{24}$$

where V_i is the volume of pore body i, S_i^α is the saturation of phase α in pore body i, and Q_{ij}^α is the volumetric flux of phase α through pore i.

Capillary pressure

The saturation of a pore body is a function of the local capillary pressure. The relationship between local capillary pressure and wetting phase saturation for cubic pore bodies is given by:

$$p_i^c(S_i^w) = \frac{2\sigma^{nw}}{R_i(1 - e^{-6.83 S_i^w})} \tag{25}$$

The derivation of this equation is given by Joekar-Niasar et al. (2010). Once a pore throat is invaded by the non-wetting fluid, a capillary pressure should be assigned to the pore throat. The capillary pressure assigned to the pore throat equals the capillary pressure of the upstream pore body.

Minimum wetting phase saturation in a pore body

Since it is impossible to completely remove the wetting phase from the corners of a pore body, each pore has a residual saturation. The minimum saturation of a pore body is assumed to be related to the global capillary pressure. The global capillary pressure is set as the capillary pressure at the inlet pores. The minimum saturation is reached when the capillary pressure in a pore body reaches the global capillary pressure. Therefore, the capillary pressure in a pore body cannot exceed the global capillary pressure. Since the Navier-Stokes equations are solved in the non-wetting reservoir, the pressure in the reservoir varies in both space and time. Therefore, the capillary pressure is also different for each inlet pore. The maximum capillary pressure is only defined for pores that are

invaded and is set as the maximum capillary pressure of the inlet pore connected to the invaded pore (Figure 5). The relation between minimum saturation and maximum capillary pressure is derived from Equation 25.

$$S^w_{i,min} = -\frac{1}{6.83}\ln(1 - \frac{2\sigma^{nw}}{R_i P^c_{max}}) \tag{26}$$

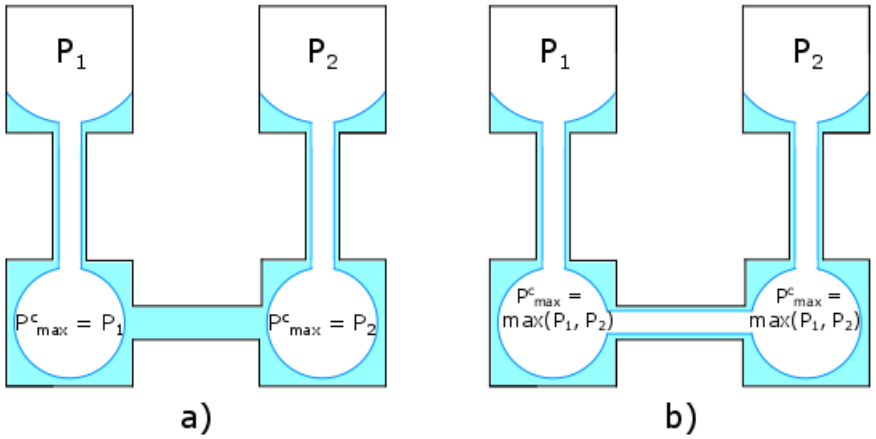

Figure 5: Maximum capillary pressure. The top pores are the inlet pores. a) The maximum capillary pressure in the pores is equal to the capillary pressure in the connected pores. b) The throat between the bottom pores is now invaded. The maximum capillary pressure in the bottom pores is now equal to the maximum capillary pressure of both inlet pores.

When the saturation of a pore body becomes lower than the local minimum saturation, it is set explicitly to the local minimum saturation. This can lead to some small errors in the mass balance. The pressure at the inlet pores also changes over time. This leads to jumps in the minimum saturation of a pore body. If the capillary pressure increases, the local minimum saturation will decrease. This will not lead to any problems. However, if the capillary pressure decreases, the minimum saturation increases. This leads to some jumps in saturation and larger errors in the mass balance. It is to be seen if this error is significant, e.g. by comparison with fully implicit models.

Entry capillary pressure for pore throats

A pore throat will be invaded by the non-wetting phase once the capillary pressure in an adjacent pore becomes larger than the entry pressure of the pore throat. The entry pressure of a pore throat with a square cross section is defined by (Ma et al., 1996):

$$p^c_{e,ij} = \frac{\sigma^{nw}}{r_{ij}}\left(\frac{\theta + \cos^2\theta - \frac{\pi}{4} - \sin\theta\cos\theta}{\cos\theta - \sqrt{\frac{\pi}{4} - \theta + \sin\theta\cos\theta}}\right) \tag{27}$$

Conductivity of pore throats

The conductivity of a pore throat depends on the throat radius and the fluid occupancy. Two situations can occur.

1. The pore throat is only occupied by the wetting phase. The expression for the conductivity is then defined as (Azzam and Dullien, 1977):

$$K^w_{ij} = \frac{\pi}{8\mu^w l_{ij}}(r^{eff}_{ij})^4 \tag{28}$$

$$K^n_{ij} = 0 \tag{29}$$

where μ^w is the dynamic viscosity of the wetting phase, l_{ij} is the length of the pore throat and

$$r_{ij}^{eff} = \sqrt{\frac{4}{\pi}} r_{ij} \tag{30}$$

2. The pore throat is invaded by the non-wetting phase and thus both phase may be present. The conductivities are then defined as (Ransohof and Radke, 1988):

$$K_{ij}^{w} = \frac{4-\pi}{\beta \mu^{w} l_{ij}} (r_{ij}^{c})^4 \tag{31}$$

$$K_{ij}^{n} = \frac{\pi}{8\mu^{n} l_{ij}} (r_{ij}^{eff})^4 \tag{32}$$

where

$$r_{ij}^{c} = \frac{\sigma^{nw}}{p_{ij}^{c}} \tag{33}$$

and

$$r_{ij}^{eff} = \frac{1}{2}\left(\sqrt{\frac{r_{ij}^2 - (4-\pi) {r_{ij}^{c}}^2}{\pi}} + r_{ij} \right) \tag{34}$$

and β is a resistance factor which depends on the roughness and geometry of the pore throat (Zhou et al., 1997).

Snap-off

If the local capillary pressure in a pore throat becomes smaller than a critical value, the corner interfaces will become unstable and the pore will be filled with only the wetting phase again. The non-wetting phase becomes disconnected as it recedes in the neighboring pore bodies. This process is called snap-off and is schematically shown in Figure 6. While snap-off is not expected to be an important process during drainage (Joekar-Niasar, 2010), it is still included in the model. The critical capillary pressure is defined as (Vidales et al., 1998):

$$p_{ij}^{c} \leq \frac{\sigma^{nw}}{r_{ij}} \big(\cos\theta - \sin\theta \big) \tag{35}$$

Snap-off will disconnect the non-wetting phase and the pore throat will be filled by the wetting phase again.

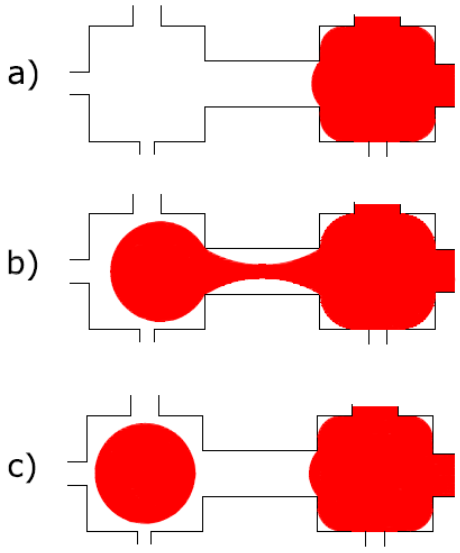

Figure 6: Schematic representation of snap-off during drainage (Joekar-Niasar, 2010).

Computational procedure

A certain non-wetting phase pressure is specified which is applied to the inlet pores. At the inlet pores, the wetting pressures is assumed to be zero. Therefore, the capillary pressure equals the non-wetting pressure. For each pore throat, the conductivity for the phases is calculated. Then the non-wetting volumetric flux can be calculated through each pore. Then, Equation 36 is used to calculate the wetting phase pressure. Using Equation 21, the non-wetting phase pressure is written as a function of the wetting phase pressure and the capillary pressure. The following set of linear equations is obtained and solved for the wetting pressure.

$$\sum (K_{ij}^w + K_{ij}^n)(P_i^w - P_j^w) = \sum K_{ij}^n (P_i^c - P_j^c) \tag{36}$$

The timestep size is important for dynamic pore-network models. When the timestep size is too large, the model will become numerically unstable. Also, the timestep must end when a pore has reached its minimum or maximum saturation. Therefore, a local time step is calculated for each pore body based on the time required to fill or drain a pore body.

$$\Delta t_i = -\frac{V_i}{Q_i^n}(S_i^w - S_{i,min}^w) \text{ for local drainage, } Q_i^n < 0 \tag{37}$$

$$\Delta t_i = \frac{V_i}{Q_i^n}(1 - S_i^w) \text{ for local imbibition, } Q_i^n > 0 \tag{38}$$

The global time step is set equal to the smallest local time step. When the time step taken is too large, the model can become unstable. In order to keep the model stable, a fraction of the smallest local time step is taken for the global time step.

Using Equation 36, the wetting phase saturation for the new time step can be calculated. Then, the saturation and capillary pressure for the next timestep can be solved explicitly according to Equations 37 and 38, and Equation 25. The non-wetting phase pressure can be calculated according to Equation 21. Once a pore has become completely saturated during local imbibition, the local non-wetting and capillary pressure are set to zero.

3.1.3 Interface

The coupling conditions between the freeflow model and the pore-network model will now be discussed. In both the free flow domain and porous medium, isothermal single-component flow is considered. Therefore, only momentum transfer across the interface is considered. Mechanical equilibrium is assumed: both the normal stresses and shear stresses must be equal in the pore-network at the interface. As a starting point, the momentum balance will be used:

$$\rho\left(\frac{\partial \bar{v}}{\partial t} + \bar{v} \cdot \nabla \bar{v}\right) = \nabla \cdot \bar{\bar{\sigma}} + \rho \bar{g} \tag{39}$$

We assume that the system is time-independent and that flow is laminar. Therefore, the time-derivative and inertial term can be neglected. Additionally, the effect of gravity at the interface is assumed to be negligible. The momentum balance then reduces to:

$$\nabla \cdot \bar{\bar{\sigma}} = \bar{0} \tag{40}$$

Two box-shaped control volumes are considered at the interface; one is located in the freeflow domain and the other one in the pore-network model (Figure 7). The divergence of the stresses integrated over the control volume can be written as the stresses multiplied by the normal vector integrated over the faces of the control volume according to Gauss' theorem.

$$\int_V \nabla \cdot \bar{\bar{\sigma}} \; dV = \int_\Gamma \bar{\bar{\sigma}} \cdot n \; d\Gamma = \bar{0} \tag{41}$$

The surface integral at the interface must be equal in both the freeflow domain and pore-network model. Thus:

$$\left[\bar{\bar{\sigma}} \cdot \bar{n}\right]^{ff} = \left[\bar{\bar{\sigma}} \cdot \bar{n}\right]^{pnm} \tag{42}$$

where the superscript ff and pnm denote the freeflow and pore-network domain, respectively. Using the expression for the stress from Equation 2, Equation 42 can be written as:

$$\bar{\bar{\sigma}} \cdot \bar{n} = \left(\bar{\bar{\tau}} - p\bar{\bar{I}}\right) \cdot \bar{n} = \left[\mu\nabla\left(\bar{\bar{v}} + \bar{v}^T\right) - p\bar{\bar{I}}\right] \cdot \bar{n} \tag{43}$$

The stress at the interface can be divided into its normal and tangential component. First, the normal component will be considered.

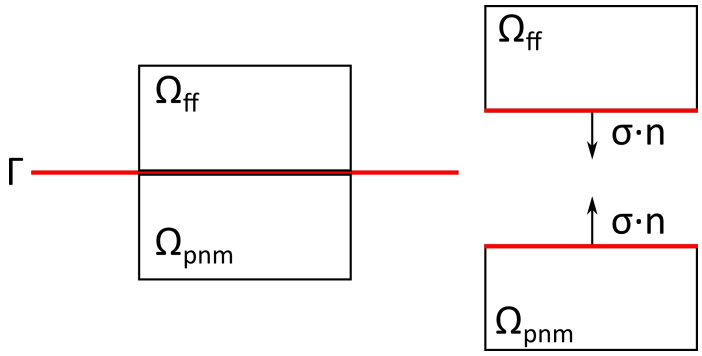

Figure 7: A control volume in the freeflow domain and a control volume in the pore-network domain are considered at interface Γ. Since both surfaces lie at the interface, the stresses at the surface of the control volumes at the interface must be equal in both domains.

3.1.3.1 Normal stress

To obtain the normal component of the stress at the interface, Equation 43 is multiplied by the normal unit vector:

$$\left(\left(\mu\nabla\left(\bar{\bar{v}} + \bar{v}^T\right) - p\bar{\bar{I}}\right) \cdot \bar{n}\right) \cdot \bar{n} = 2\mu\frac{\partial v_z}{\partial z} + p \tag{44}$$

This term must be equal on both sides of the interface:

$$\left[2\mu\frac{\partial v_z}{\partial z} + p\right]^{ff} = \left[2\mu\frac{\partial v_z}{\partial z} + p\right]^{pnm} \tag{45}$$

However, flow in the pore-network model is considered to be one-dimensional. The flow within a pore throat is constant and does not change over the length of the pore throat. Thus, the viscous stress term disappears for the pore-network model and the following condition is obtained:

$$\left[2\mu\frac{\partial v_z}{\partial z} + p\right]^{ff} = \left[\ p\ \right]^{pnm} \tag{46}$$

This leads to a discontinuity in pressure, while pressure normally is a continuous property. The significance of this pressure jump will be investigated in this study.
In the case of two-phase flow, the pores at the interface are only filled with air. Therefore, only the forces between air in the freeflow domain and air in the pore need to be considered. The following is condition for the normal stress for is then obtained for a two-phase flow situation:

$$\left[2\mu^n\frac{\partial v_z^n}{\partial z} + p^n\right]^{ff} = \left[p^n\right]^{pnm} \tag{47}$$

where the superscript n denotes the non-wetting phase.

3.1.3.2 Shear stress

For the shear stresses at the interface, the Beavers-Joseph condition is used in the freeflow domain. The use of the Beavers-Joseph condition in this case is questionable, because it is a macroscale condition, while the pore-network model describes flow at the pore scale. The Beavers-Joseph relation uses the intrinsic permeability of the porous medium, which is not defined at the pore-scale. Nevertheless, it is used as a boundary condition for the freeflow domain. Because the pore-throats are

aligned perpendicular to the interface, the horizontal flow velocity is 0 in the pore-network model. Therefore, the Beavers-Joseph-Saffman slip-condition is used (Beavers and Joseph (1967), Saffman (1971)). which is a special case of the Beavers-Joseph condition where the tangential velocity in the porous medium equals 0. This is schematically shown in Figure 8.

$$\left[\left(v - \frac{\sqrt{K_i}}{\mu\alpha_{BJ}}\tau \cdot n\right) \cdot t_i\right]^{ff} = 0 \tag{48}$$

This equation can be used for both single-phase and two-phase flow.

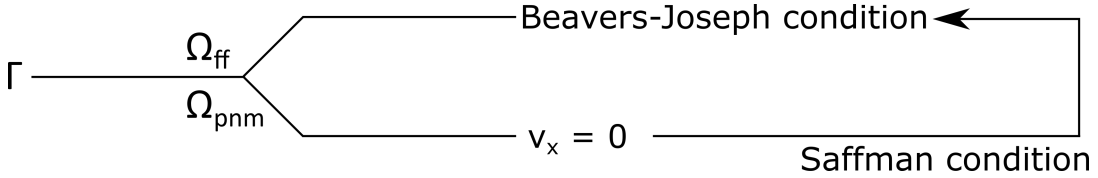

Figure 8: For the freeflow domain, the Beavers-Joseph condition is used. In the pore-network, no tangential flow is assumed. This justifies the use of the Beavers-Joseph-Saffman condition

3.1.3.3 Mass flux

Furthermore, continuity of mass flux is assumed. Thus, the mass flux in the porous medium should equal to mass flux in the free flow domain at the interface. Hereby, it is assumed that the pore throats are aligned perpendicularly to the interface. For single-phase flow, continuity of mass can be expressed as:

$$\Big[\rho v \cdot n\Big]^{ff} = \Big[\rho v \cdot n\Big]^{pnm} \tag{49}$$

This condition can also be used for two-phase flow in the pore-network model, because only the non-wetting phase is allowed to leave or enter the pore-network. Therefore, only the mass flux of the non-wetting phase has to be considered:

$$\Big[\rho^n v^n \cdot n\Big]^{ff} = \Big[\rho^n v^n \cdot n\Big]^{pnm} \tag{50}$$

where the superscript n denotes the non-wetting phase.

3.1.3.4 Implementation

Here, the implementation of the aforementioned coupling conditions will be discussed. The coupling conditions can be used for both a Dirichlet coupling or Neumann coupling. The Dirichlet coupling uses Equation 46 as a Dirichlet condition for the pressure at the interface in the pore-network model. Equation 49 is used as a Dirichlet condition for the normal velocity in the free flow domain along the interface. For Neumann coupling, Equation 46 is used as a Neumann condition for the velocity in the freeflow domain. Equation 49 is used as a Neumann condition for the pore-network model. Both options have been investigated. However, the Neumann coupling is unstable, because small pressure differences between the models leads to large velocity gradients. If the velocity gradient becomes too large, the model will not converge. The Dirichlet coupling is stable and is therefore the major focus point in this study. Pores at the top of the pore-network are assumed to lie in the freeflow domain. Because flow is assumed to go from the freeflow domain in to the pore-network, these pores are from here on referred to as the inlet pores. The inlet pores only have one connection per pore and are connected to the pores directly below them. They are not connected laterally, because these pores lie in the freeflow domain and lateral flow is solved in the Stokes domain. Therefore, there is no flow directly between the inlet pores. The same applies to the bottom pores, except that they are only connected to the pores directly above them. Now, the boundary conditions at the interface will be discussed for both single-phase and two-phase flow.
The free flow model and the pore-network model are coupled iteratively. First, Stokes equation is solved in the free flow domain using velocity data obtained from the pore-network model. For the first iteration, the data from the solution of the previous timestep is taken. Then, data from the

free flow domain along the interface is obtained and passed to the pore-network model, which is then solved. Then, the velocity along the interface resulting from the pore-network model is compared to the previous velocity along the interface. If the change in normal velocity is smaller than a specified tolerance threshold, the next timestep will be started. If the change in velocity is too large, the free flow domain will be solved again with the updated normal velocity boundary condition.

Single-phase model

At the top and bottom boundaries, a no-flow condition is used, except at the location of the interface. At the interface, the velocity in the inlet throats is used as a boundary condition for the normal velocity in the freeflow domain. The Beavers-Joseph-Saffman equation is used for the tangential velocity. The pressure in the inlet pores is set to the normal stress at the interface in the freeflow domain, consisting of the pressure and viscous stress. At the outlet pores, either the pressure is fixed or a no-flow condition is used.

Two-phase model

At the interface, the velocity of the non-wetting phase in the inlet throats is used as a boundary condition for the normal velocity in the freeflow domain. The Beavers-Joseph-Saffman equation is used for the tangential velocity. The non-wetting phase pressure in the inlet pores is set to the normal stress at the interface in the freeflow domain. The wetting phase pressure is set to zero in the inlet pores, because there is no wetting phase present in the freeflow domain. The capillary pressure then equals the non-wetting phase pressure in the inlet pores. At the outlet pores, the wetting phase pressure is set to zero. No wetting fluid is allowed to enter the freeflow domain. Therefore, the wetting-phase conductivity of the inlet throats is set to zero. The reverse is used for the outlet throats: no non-wetting fluid is allowed to enter the wetting reservoir and the non-wetting conductivity of the outlet throats is set to zero. Both the top and bottom pores are not included into the calculation of the total saturation. The maximum allowed capillary pressure is set as the maximum capillary pressure at the inlet. The wetting phase pressure in the top pores is set to zero, as no wetting phase is present in the freeflow domain. The Beavers-Joseph condition is used as a Dirichlet condition for the horizontal flow velocity in the free flow domain along the interface. A Dirichlet condition is also used for the vertical flow velocity along the interface. To obtain the velocity from the pore-network model, the volumetric discharge through the pore throats is divided by the cross-sectional area of the throat. The flow velocities of all throats in a cell are averaged by their area and assigned to the respective cell of the free flow domain. A schematic representation of the interface is shown in Figure 9.

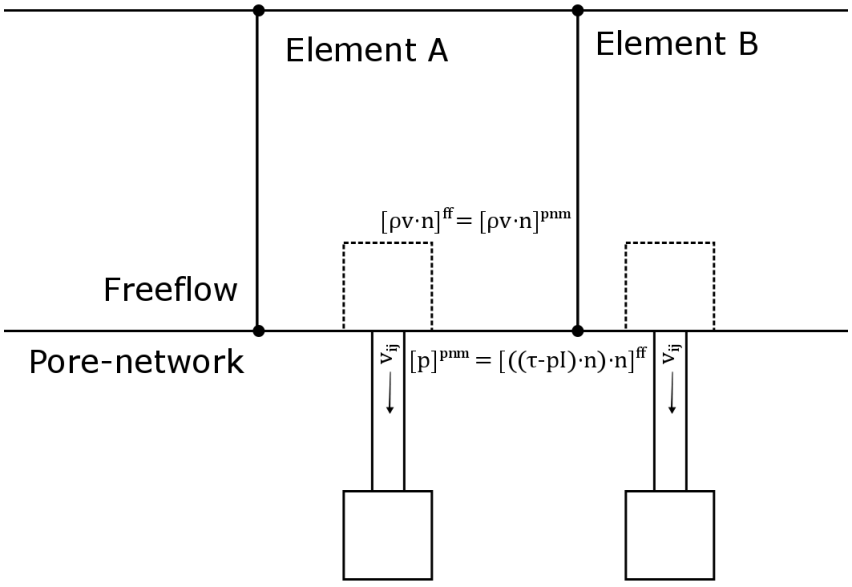

Figure 9: Schematic representation of the interface between free flow and pore-network model.

3.1.4 Boundary conditions and parameters

The pore network is based on the micromodel, which will be discussed in the next section. The network is a regular grid, with 16, 16 and 1 pores in the x, y and z-directions respectively. The inlet pores are not connected with each other. The same applies to the outlet pores. All pore bodies have the same radius. At the outlet pores, either a Dirichlet condition is used for the pressure, or a no-flow condition is used. The used pore sizes are shown in Table 1.
The freeflow domain consists of a 2-dimensional rectangular grid. At the left boundary, the horizontal flow velocity is set as a Dirichlet condition. A fixed horizontal velocity profile is set at the left boundary of the freeflow domain.

$$v_x = v_0 \frac{y - y_{min}}{0.25(y_{max} - y_{min})^2} \tag{51}$$

Therefore, only the value of v_0 has to be specified at the left boundary. At the top and bottom boundaries a no-flow condition is used, except at the location of the interface. An outflow condition is used for the pressure, and its value is set as a Dirichlet condition at the right boundary. The domain is discretized in square grid cells. The Stokes equation is solved using the Box method (Huber and Helmig, 2000). The pressure at the right-hand side of the freeflow domain is set to 10^5 Pa. The Beavers-Joseph-Saffman condition (Equation 14) is used as a Dirichlet condition for the horizontal flow velocity in the free flow region at the interface. The macroscopic intrinsic permeability of the porous medium in the flow direction in the freeflow domain is therefore required. It is obtained through numeric upscaling: in a separate pore-network model, a pressure difference is induced between the left- and right-hand sides of the network. The volumetric flux at the outlet is calculated. By rearranging Darcy's Law, the intrinsic permeability can be obtained through the following equation:

$$\kappa = \frac{\mu Q}{A \frac{\Delta P}{\Delta x}} \tag{52}$$

where Q is the volumetric discharge at the outlet and A is the cross-sectional area at the outlet. The resulting values for permeability are shown in Table 1. Properties for both the single-phase and two-phase models are given in Table 2.

Pore body radius [m]	**Pore throat radius [m]**	**Upscaled intrinsic permeability** $[m^2]$
$1.25 \cdot 10^{-4}$	$3.40 \cdot 10^{-5}$	$1.27 \cdot 10^{-11}$
$1.25 \cdot 10^{-4}$	$1.25 \cdot 10^{-4}$	$2.32 \cdot 10^{-9}$

Table 1: Intrinsic permeability for pore-networks with various pore sizes.

Property	**Symbol**	**Value**	**Units**
Density of water	ρ_{water}	$1.0 \cdot 10^3$	kg/m^3
Viscosity of water	μ_{water}	$1.0 \cdot 10^{-3}$	$Pa\ s$
Density of water	ρ_{air}	1.2	kg/m^3
Viscosity of water	μ_{air}	$1.82 \cdot 10^{-5}$	$Pa\ s$
Contact angle	θ	0	$^\circ$
Air-water interfacial tension	σ	0.072	kg/s^2
Throat shape factor	β	100	-

Table 2: Fluid and pore-network properties used in the pore-network models.

3.2 Experiments

The interaction between free flow and porous media has also been studied experimentally. For this purpose, a micromodel has been constructed which contains a free flow domain and a porous medium domain. The model is investigated using confocal microscopy. In confocal microscopy, light will have to travel through a screen with a pinhole. This eliminates the out-of-focus light and allows for acquisition of high resolution images. The velocity field can be determined by particle tracking. In this section, details about the microscope, the micromodel and the experimental setup will be given.

The scanners run at 24 frames per second with a resolution of 2.47 μm. The microscope is able to track particles in 3 dimensions. Three-dimensional flow inside a pore body or throat is not solved in a pore-network model and the porous medium region of the pore-network model consists of only one pore in the z-direction. Therefore, the z-direction is omitted and only the two-dimensional velocity field has been determined.
The micromodel is fabricated by laser cut technique from silicon glass. Silicon gasket has been used for sealing and a thin glass layer of 50 μm thickness is used for covering the porous medium section. The micromodel consists of two major components: the free flow domain and the porous structure (Figure 10). The porous structure is 1 cm by 1 cm and is filled with glass columns. The mean pore size is 250 μm. A capillary tube is attached at the bottom of the porous medium, to serve as a drain for the water present in the porous medium. The structure has a depth of 500 μm. The free flow domain is a capillary tube. The length of the tube leading up to the porous medium is 16 cm, in order to achieve a fully-developed velocity profile. The tube has a square cross-section. Both the height and depth of the tube are 500 μm.

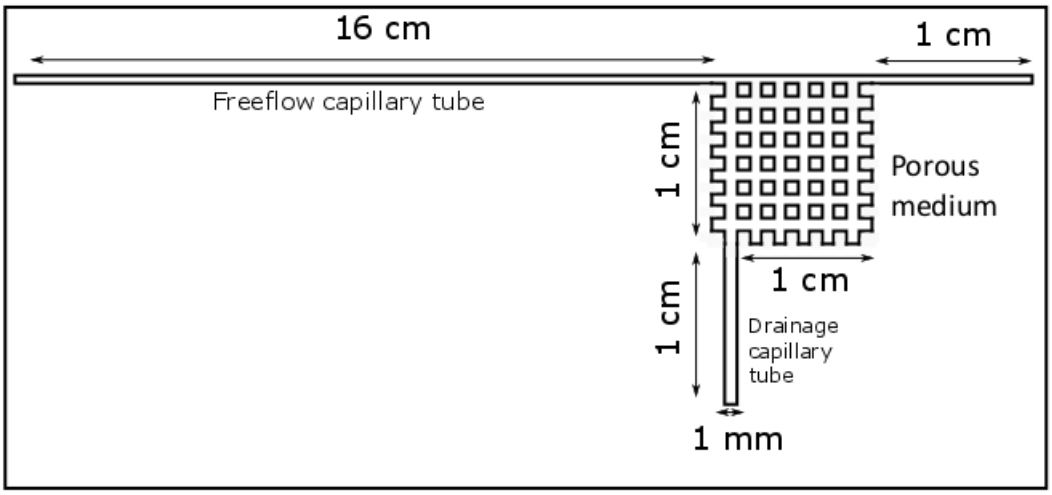

Figure 10: Schematic representation of the micromodel.

In order to make a meaningful comparison with the numerical model, the flow in the freeflow region must be laminar. Therefore, the Reynolds number must be known. For a pipe with a square cross-section, the Reynolds number can be calculated as :

$$Re = \frac{\rho D Q}{\mu A} \tag{53}$$

where ρ is the fluid density, Q is the volumetric flow rate of the fluid, μ is the dynamic viscosity of the fluid and A is the cross-sectional area of the pipe. D is the hydraulic diameter and is defined as:

$$D = \frac{4A}{P} \tag{54}$$

P is the wetted perimeter, which is defined for a square cross-section as:

$$P = 2(L_x + L_y) \tag{55}$$

Property	Symbol	Value	Units
Density of water	ρ_{water}	$1.0 \cdot 10^3$	kg/m^3
Viscosity of water	μ_{wwater}	$1.0 \cdot 10^{-3}$	Pas
Density of water	ρ_{air}	1.2	kg/m^3
Viscosity of water	μ_{air}	$1.82 \cdot 10^{-5}$	Pas
Characteristic length	L	$5.0 \cdot 10^{-4}$	m
Cross-sectional area	A	$2.5 \cdot 10^{-7}$	m^2

Table 3: Fluid and micromodel properties used for the calculation of the Reynold's number.

The parameters used in the calculation of the Reynold's number are shown in Table 3. The porous medium is initially saturated with water. Then, water is injected in the freeflow capillary tube. The water contains fluorescent particles which can be tracked to determine the velocity field. The velocity of the particles is assumed to be equal to the velocity of the water. At each frame, a particle gives data about the velocity at that position. These data points are then interpolated using the griddata function in Matlab to obtain the velocity field. The Beavers-Joseph coefficient can be determined from Equation 13, if the velocity field is known. The intrinsic permeability of the porous medium could not be determined experimentally. Therefore, it is estimated by numeric upscaling, as mentioned in the previous section.
In the case of two-phase flow, the porous medium will be initially filled with water. Air is injected in the freeflow capillary tube with a specified flow rate, using a flow meter. The water contains fluorescent particles which can be tracked to determine the flow velocity. The water is also colored, which allows for a contrast between the air and water phase. Thus, the air-water interface can be visualized. There are no particles placed in the air. The flow velocity of the air is very large relative to the flow velocity of water. It is expected that the particles in the air would move too fast for particle tracking. The flow rates which have been used and their corresponding Reynold's number are shown in Table 4 for both the single-phase and two-phase experiments.

Water	**Q [L/min]**	**Re [-]**
	$0.1 \cdot 10^{-3}$	3.3
Air	**Q [L/min]**	**Re [-]**
	0.4	$8.8 \cdot 10^2$
	0.6	$1.3 \cdot 10^3$
	1.0	$2.2 \cdot 10^3$

Table 4: Volumetric flow rates used in the experiments. with corresponding Reynold's numbers.

4 Results and discussion

The results from the simulations and experiments mentioned in the previous section will now be presented. The simulation results are focused on convergence of the model and the significance of the pressure discontinuity will be discussed. Then, the results of the experiments will be presented, which is focused on the velocity field and Beavers-Joseph coefficient. Afterwards, the results of the experiments and simulations are compared.

4.1 Simulations

4.1.1 Single-phase freeflow and single pore-network model

4.1.1.1 Convergence

Since the coupling is done iteratively, it might take a large amount of iterations before a solution is reached. A timestep converges if the change in normal velocity at the interface is smaller than a specified absolute tolerance. This value is set at $1 \cdot 10^{-12}$ m/s. The model does not converge in all situations. The Stokes model has trouble converging when there are large spatial variations in flow velocity. These variations lead to large pressure gradients, creating unrealistically large pressures in the free flow domain. Large flow velocities can be introduced by the Dirichlet boundary conditions for the horizontal and vertical flow velocity along the interface. The vertical flow velocity is determined by the flux through the pore throats at the interface. Large pore throat radii or small throat lengths lead to high flow rates because of the low resistances to flow. If these parameters are too large, the model will not converge. The pore throat velocity is defined as:

$$v = \frac{Q}{A} \tag{56}$$

The volumetric discharge Q is a function of the pore throat radius to the power of 4, while the area of the pore throat is a function of the throat radius to the power of 2. Thus, the volumetric discharge Q increases stronger for a larger throat radius than the throat area and the throat velocity increases with increasing throat radius.
The horizontal flow velocity is determined by the Beaver-Joseph coefficient, which will be further discussed in the next section. The amount of coupling iterations required before a solution is reached ranges from 1 to 10. At the start, a larger amount of iterations is required. The amount of iterations decreases as less changes occur in the velocity and pressure fields and the model approaches a steady-state. For velocities of 0.05 m/s in the freeflow domain, only 1 to 3 iterations are required, while for flow velocities of 1.0 m/s, 1 to 10 iterations are required before a solution is obtained. The model has also been run with air as the fluid. Air has a lower viscosity than water. This leads to larger velocities at the interface. More coupling iterations are required before a solution is reached. Furthermore, the convergence of the model depends on the size of the timestep. For larger timesteps, the amount of coupling iterations will increase and the Stokes model has trouble converging. The Stokes model will not converge if the timestep is too small, which is $1 \cdot 10^{-7}$ s for water. When using air as the freeflow fluid, the model will converge poorly and pressure oscillations exist in the freeflow domain. For larger timestep sizes, the Stokes model converges fine. Thus, the timestep size should be larger than $1 \cdot 10^{-7}$ s. In the following sections, the network with throat radii of $3.4 \cdot 10^{-5}$ m has been used, as this led to the best convergence. Thus, the results shown in this section are not obtained with the same pore sizes as the micromodel.

4.1.1.2 Flow patterns

Flow in the Stokes domain is from left to right under standard conditions, when no pore-network is attached. If a pore-network is attached to the freeflow model, the resulting flow is dependent on the boundary condition imposed on the outlet pores of the pore-network model. If a fixed boundary conditions is set in the outlet pores, the flow is mainly in vertical direction. If a no-flow condition is used at the outlet, a circulation of water occurs in pore-network (Figure 11). The largest flow velocities in the pore-network occur near the interface. The velocity decreases further away from the interface. The flow pattern is in agreement with the pressure field for both situations (Figure 12). In the modelled scenarios, water is leaving the Stokes domain and enters the pore-network. If the amount of water leaving the Stokes domain over the interface becomes too large, water will flow from

the right-hand boundary of the Stokes domain towards the pore-network. Thus, water will flow from both the left and right-hand boundaries towards the interface.

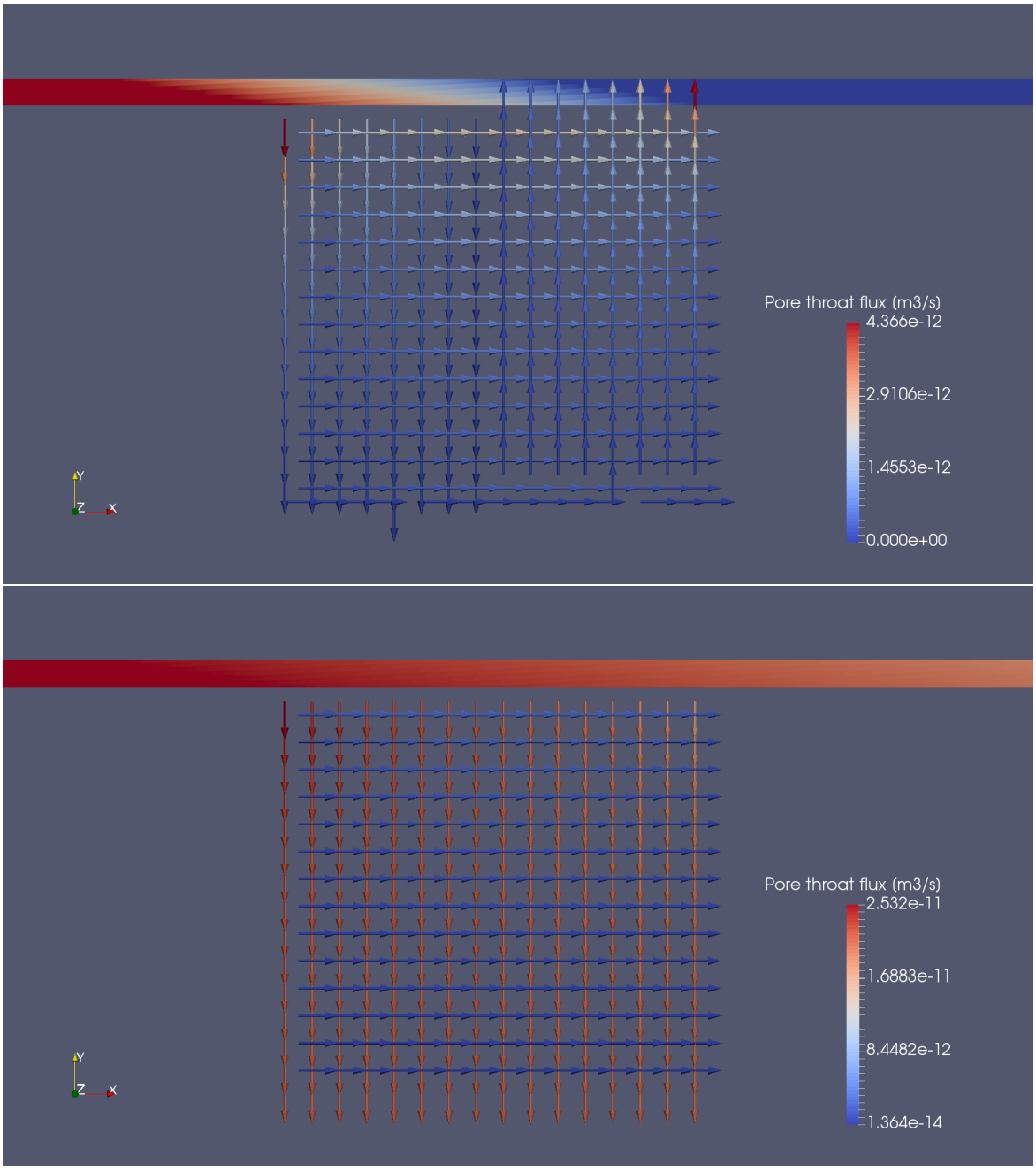

Figure 11: Flow direction in pore throats for two situations: no-flow condition at the bottom and a fixed pressure at the bottom.

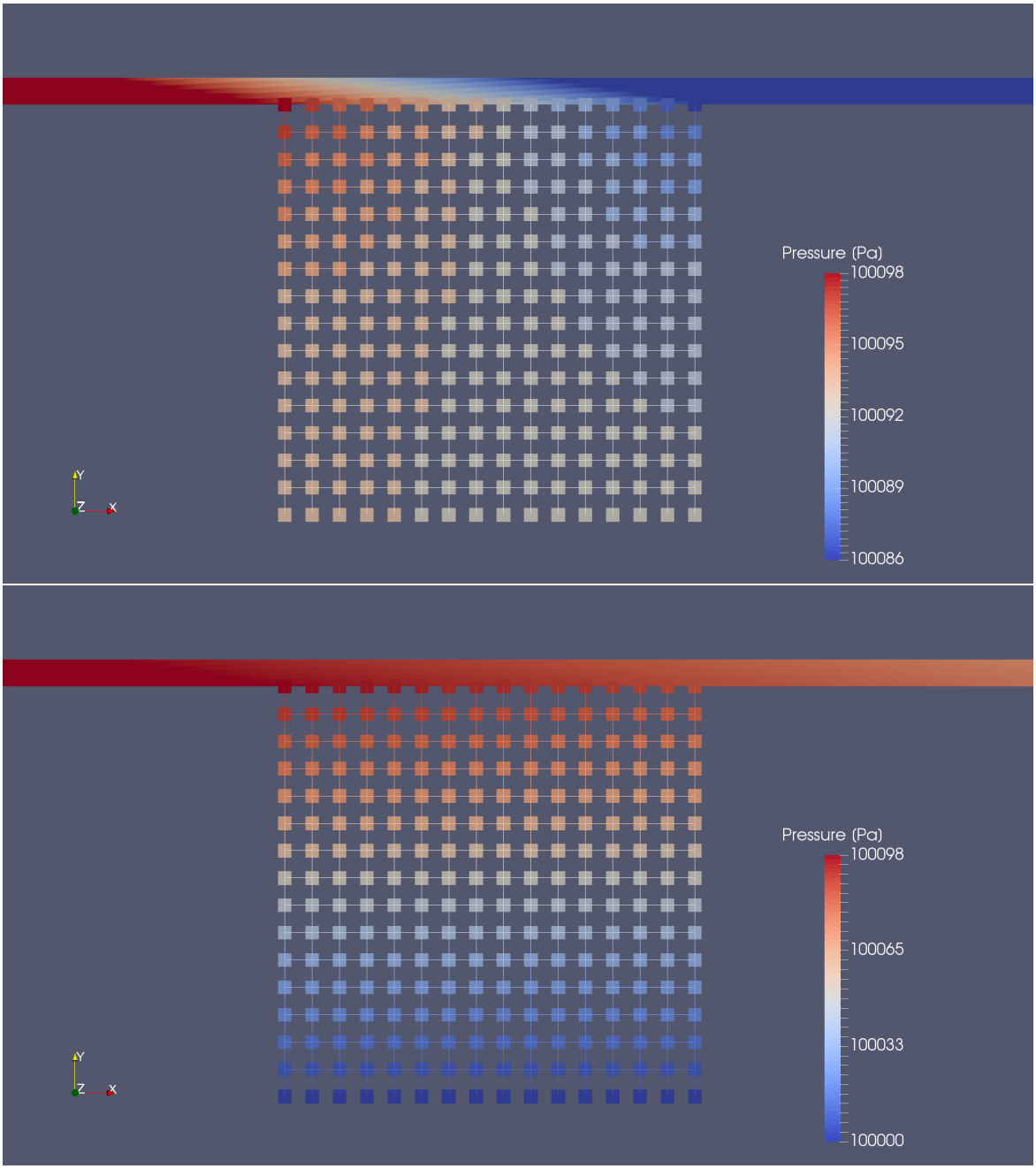

Figure 12: Pressure field for two situations: no-flow condition at the bottom and a fixed pressure at the bottom.

4.1.1.3 Beavers-Joseph coefficient

The Dirichlet boundary condition for the horizontal flow velocity at the interface depends on the value chosen for the Beavers-Joseph coefficient α_{BJ}. Large flow velocities occur when small values for the Beavers-Joseph coefficient are used. This leads to large velocity gradients and therefore pressure differences in the free-flow domain. If the pressure differences become too large, the free-flow model will stop converging. Therefore, there is a limited range of usable values for the Beavers-Joseph coefficient. Since both α_{BJ} and κ are constants, this threshold depends on both parameters. When $\frac{\sqrt{\kappa}}{\alpha_{BJ}}$ becomes larger than $5 \cdot 10^{-5}$ m , the model will not converge. For an intrinsic permeability of $1.27 \cdot 10^{-11}$ m^2, the minimum value for α_{BJ} is 0.07. The horizontal flow velocity at the inlet seems to have no influence on this threshold for the Beavers-Joseph coefficient. The velocity profiles in the freeflow domain for different values for the Beavers-Joseph coefficient are plotted in Figure 13. For smaller values for the Beavers-Joseph coefficient, the velocity at the interface becomes larger, while

the velocity at the center of the channel is smaller. For larger values of the Beavers-Joseph coefficient, the velocity at the interface will be lower and the velocity profile will approach the parabolic profile set at the left boundary, described in Equation 51. Figure 13 shows that the parabolic velocity profile is approached for a value of 0.5 for α_{BJ}. Larger numbers for the Beavers-Joseph coefficient will result in similar velocity profiles, as Figure 13 shows that the difference between a value of 0.5 and 1.0 is very small. For higher values for the Beavers-Joseph coefficient, the pressure gradient along the interface becomes larger. In the case of a closed outlet, this leads to larger fluxes entering or leaving the freeflow at the interface. The difference in pore throat velocity can be up to 20% when comparing a value of 0.20 and 1.0 for α_{BJ}.

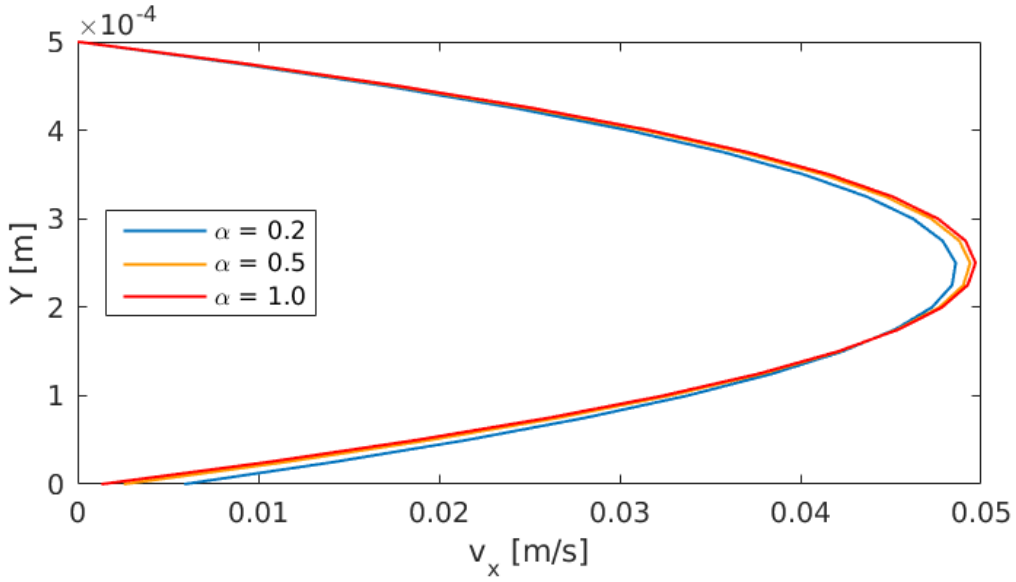

Figure 13: Effect of Beavers-Joseph coefficient for $v_0 = 0.05$ m/s. The interface with the pore-network model is located at Y = 0.

4.1.1.4 Continuity of normal stress

For the coupling conditions between the two models, continuity of normal stress is chosen at the interface. This leads to a discontinuity in pressure. Pressure is a continuous thermodynamic property at the microscale and thus this assumption is unrealistic. However, using continuity of pressure at the interface leads to a discontinuity of normal stress. In order to determine the effect and magnitude of the pressure jump, both continuity of normal stress and continuity of pressure will be investigated. The pressure jump between the freeflow domain and pore-network is equal to the viscous stress in the freeflow domain at the interface:

$$\Delta p = \left(\bar{\bar{\tau}} \cdot \bar{n}\right) \cdot \bar{n} = 2\mu \frac{\partial v_z}{\partial z} \tag{57}$$

where Δp represents the pressure jump at the interface.
The magnitude of the viscous stress at the interface was found to be small compared to the pressure. Typical values were smaller than 1 Pa. Figure 14 shows the relative magnitude of viscous forces, compared to the total normal stress at the interface. The viscous forces at the interface are very small and compromise less than $1 \cdot 10^{-4}$% of the total normal stress. Therefore, the viscous stress is negligible compared to the pressure at the interface. For higher flow rates, the viscous forces become more important, however, in the flow rates used in this study, the viscous forces and pressure jump are insignificant. For comparison purposes, the model has also been run with continuity of pressure at the interface. For low flow velocities, there is no difference at all in the velocity profile. This is due to the low viscous forces and the small pressure jump. For higher flow velocities, the pressure jump is larger. However, it is still very small and the effects on the velocity profile are negligible. Therefore, the choice of continuity of pressure or continuity of normal stress is not important in the cases investigated in this study.

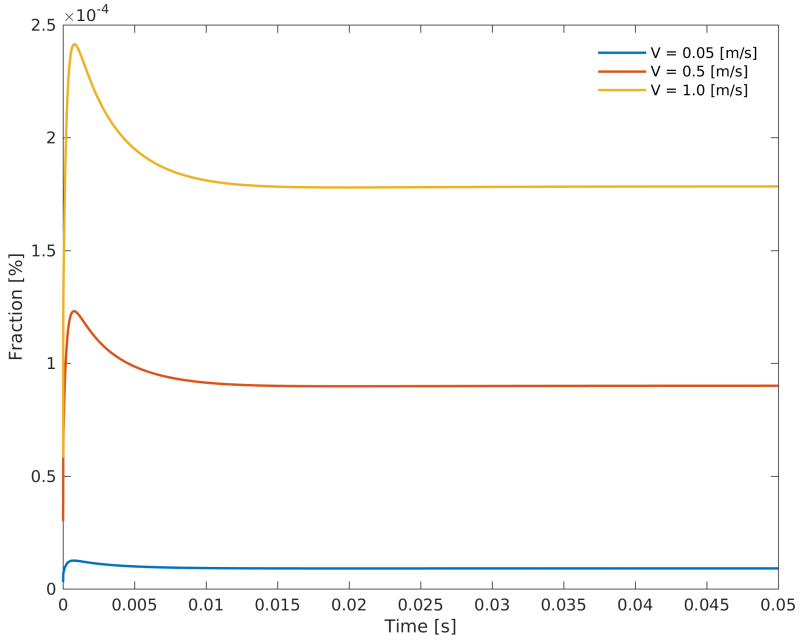

Figure 14: Relative magnitude of the pressure jump at the freeflow-porous medium interface.

4.1.2 Single-phase freeflow and two-phase pore-network model

4.1.2.1 Convergence

In this case, the freeflow domain is filled with air. The pore-network is initially saturated with water. The main difference to the single-phase model is that the timestep size must be sufficiently small for the dynamic pore-network model. The timestep size must be smaller than the largest allowed timestep size defined in Equation 37. Depending on the pore sizes, fluid properties and pressure at the inlet, the maximum allowed timestep size for the pore-network model can be in the range of 1e-7 seconds. Thus, the required timestep size is too small for the Stokes model, as mentioned in the previous section, and the model will not converge. When using larger pore sizes, the maximum allowed timestep size becomes larger, because it takes more time to drain a pore body. The model converges well when using larger timestep sizes.
The Stokes model has trouble converging. This is again caused by large gradients in the velocity. Air is used in the freeflow domain. As mentioned in the single-phase results, this leads to worse convergence of the Stokes model, compared to using water in the freeflow domain. The model only converges for small air flow rates. In this case, a value of 0.5 m/s has been used for v_0. For two phase flow, the amount of iterations can vary from 1 to over 70. For low velocities in the freeflow domain, only 1 to 3 iterations are required. For larger flow velocities, the amount of iterations can go up to 80. However, the model is unstable for high velocities and will stop converging after a certain time.

4.1.2.2 Flow field

Invasion of the pore-network is determined by the pressure at the interface. Thus, the pressure set at the right boundary of the freeflow model is the most important factor that determines if invasion will occur. If the normal stress in the freeflow region exceeds the entry pressure of the inlet throats, the pore-network will start to drain. Air enters the pore-network from the Stokes model. This air flow rates increases over time as the pore-network drains. The flow of water is directed mainly downwards, towards the wetting reservoir (Figure 15). Horizontal flow also occurs, but is 3 orders of magnitude smaller. The vertical flow rate per pore throat is $10^{-8}\ m^3/s$, the horizontal flow rate is $10^{-12}\ m^3/s$. For air, the flow rate in vertical direction is $10^{-8}\ m^3/s$ and $10^{-11}\ m^3/s$ in horizontal direction. If the pressure in the freeflow region is smaller than the inlet throat entry pressure, air will not invade the pore-network. There is no movement of water in the network in this case.

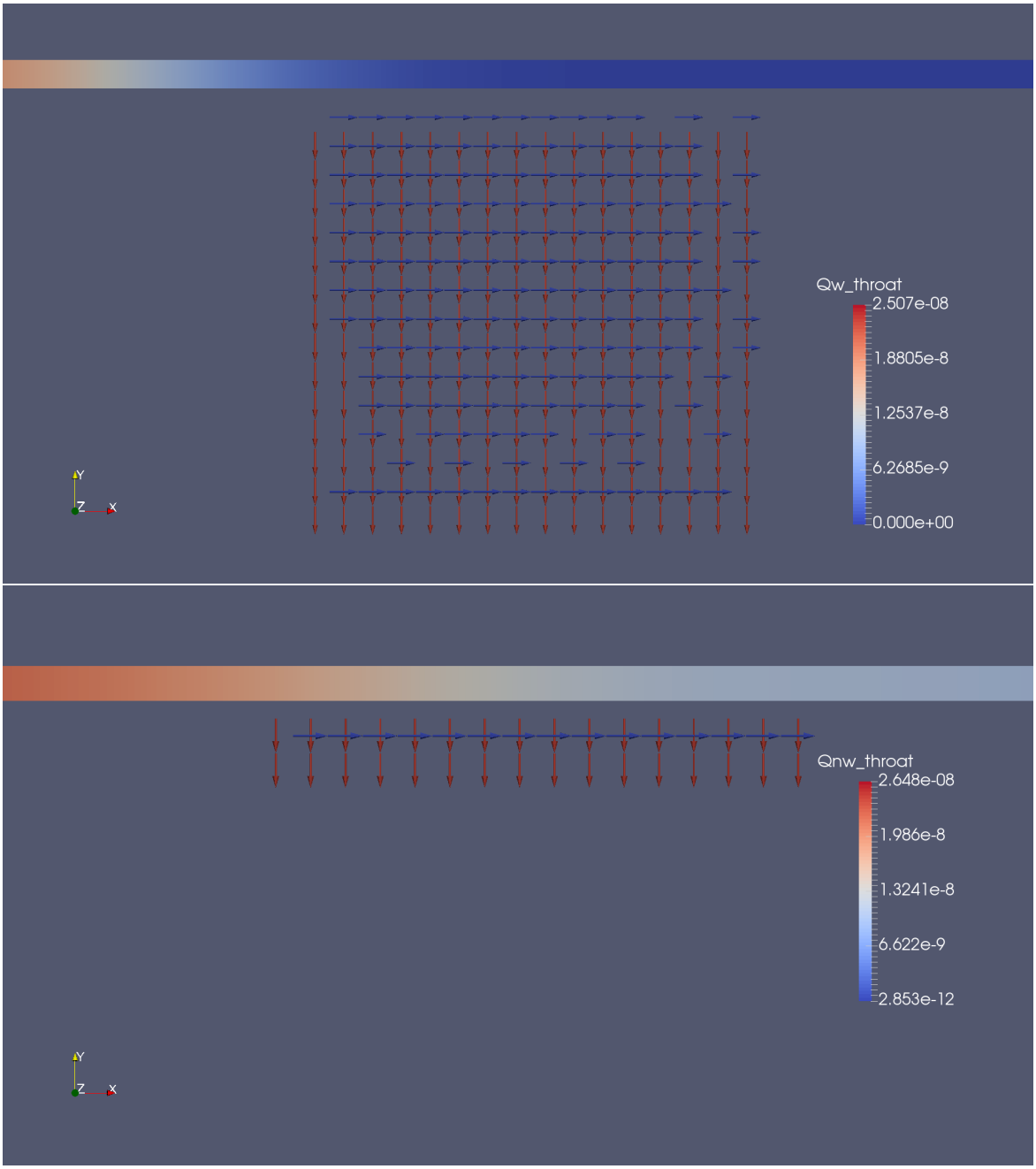

Figure 15: The flow direction and magnitude of water and gas in the pore throats is shown in the top and bottom figure, respectively. Gas pressure in freeflow domain is set to $1 \cdot 10^5$ Pa. $V_0 = 0.5$ m/s.

4.2 Experiments

The results of the experiments will be presented and discussed in this section. First, the single-phase scenario will be considered, where water occupies both the freeflow domain and the porous medium. Secondly, two-phase flow will be considered, where the freeflow domain is occupied by air and the porous medium by both air and water.

4.2.1 Single-phase freeflow and single-phase porous medium flow

4.2.1.1 Velocity field

The flow velocity has been measured in several regions in the porous medium. Both the horizontal and vertical flow velocity have been measured and averaged per pore throat. Water enters the porous

medium in the pores on the left side and flows both downwards and towards the right. Water will leave the porous medium to reenter the free flow region at the right-hand side. The observed pattern is similar to Figure 11. Figure 16 shows the velocity field and direction for the region at the right-hand side of the porous medium, near the interface. Figure 17 shows the velocity profile, taken at the transect indicated in Figure 16. At the left side of the porous medium, both the horizontal and vertical flow velocities are around 140 μm/s near the interface. At the right-hand side of the porous medium, horizontal velocities of 250 μm/s and vertical velocities of 280 μm/s have been measured. The flow velocity in the porous medium decreases with distance to the interface. At the bottom of the porous medium, the horizontal flow velocity is around 30 μm/s. Even for the highest flow velocities, the Reynolds number equals 0.06. Thus, flow is laminar in the porous medium, which supports the assumption made in the pore-network model.

It should be noted that minor leaks were present in the micromodel. Therefore, the flow velocity in the freeflow tube in the micromodel is not exactly the same as the flow rate determined from the flow meter. However, it is believed that the leakage is very small and does not influence the results significantly. Particle tracking is done automatically by the Nikon software. Some small errors in the particle tracking can occur. Furthermore, the velocity can only be measured at discrete points and is therefore interpolated to obtain the velocity field. This can introduce some errors in the measured velocity data.

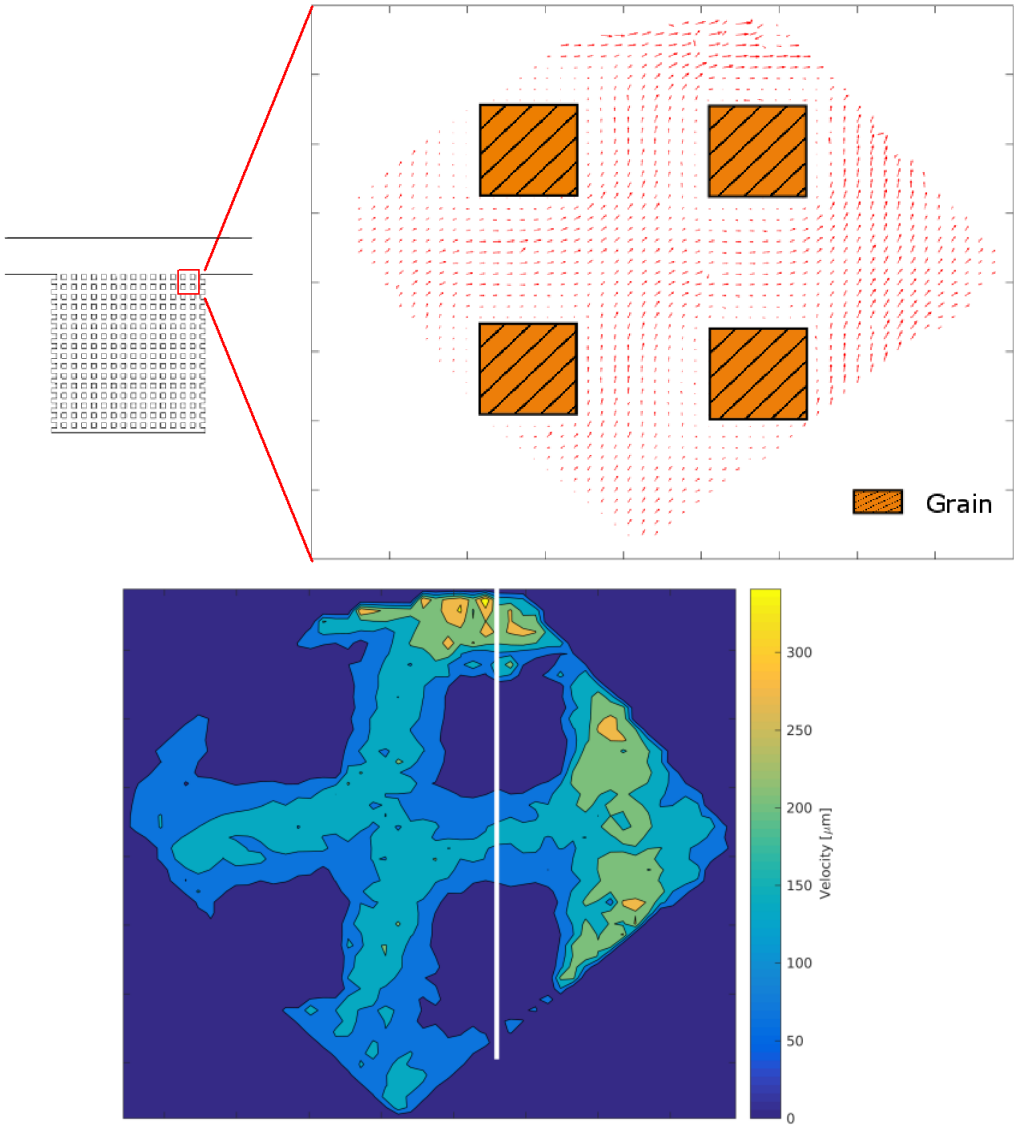

Figure 16: Velocity field obtained using particle tracking. The top graph shows the flow direction. The bottom graph shows the velocity in x-direction.

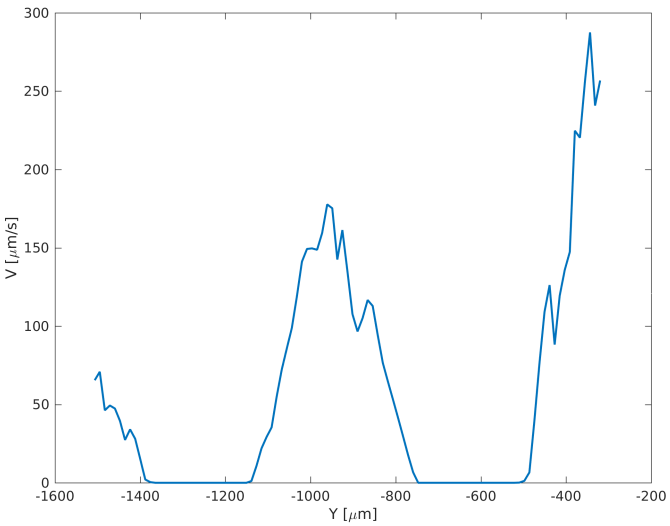

Figure 17: Profile of horizontal flow velocity, taken at the line shown in Figure 16.

4.2.1.2 Beavers-Joseph coefficient

Using the obtained velocity field, the Beavers-Joseph coefficient can be determined from Equation 13. The velocity inside the porous medium and the free flow domain are measured. The velocity gradient can be obtained from the velocity field. The intrinsic permeability of the porous medium is estimated through pore-network modeling. The value used is stated in Table 1, with a pore body and throat radius of 125 μm. The Beavers-Joseph coefficient is dependent on the geometry of the porous medium and should not depend on the flow velocity. Both the horizontal flow velocity and its gradient are spatially variable. Therefore, the velocity has been measured at several points, which leads to a dataset of multiple values for the Beavers-Joseph coefficient. The horizontal flow velocity is also measured and averaged at several areas along the interface. The distribution of the values found for the Beavers-Joseph coefficient are shown in Figure 18. A mean value of 0.51 has been found. This value is in agreement with typical values found in Beavers and Joseph (1967), which reports values in the order of 0.1 to 1.0. However, it should be noted that there is no fixed uniform pressure gradient induced in the porous medium. For the velocity in the porous medium, the constant velocity caused by this pressure gradient is taken. In this case, the tangential velocity approaches zero at further away distances from the interface. Therefore, when calculating the Beavers-Joseph coefficient, the tangential velocity is assumed to be zero. While the tangential velocity approaches zero further away from the interface, a velocity of zero is not reached at the bottom of the porous medium. Therefore, it could be argued that velocity in the porous medium should not be taken as zero. If a horizontal velocity larger than zero is chosen, the Beavers-Joseph coefficient would be larger. When the velocity in the bottom of the porous medium is taken (30 $\mu m/s$), the mean value of α_{BJ} is 0.56. For a value of 100 $\mu m/s$, which occurs in the center of the porous medium, a mean value of 0.78 for the Beavers-Joseph coefficient is calculated.

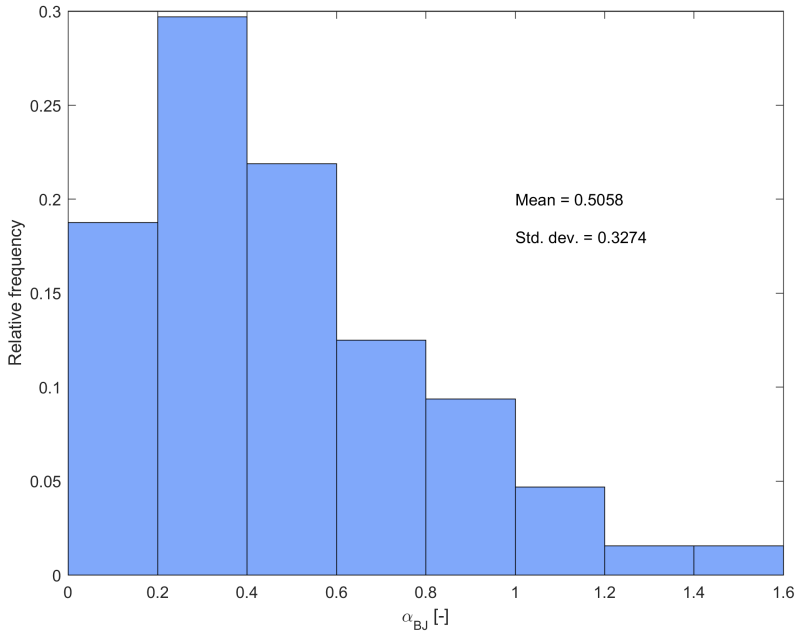

Figure 18: Distribution of values found for Beavers-Joseph coefficient from experiments.

4.2.2 Single-phase freeflow and two-phase porous medium flow

The air does not contain any fluorescent particles and the velocity field in the air cannot be determined. The water does contain particles and also contains a dye. Therefore, the air-water interface can be visualized. The air flow rate is controlled by a flow meter, where the desired volumetric flow rate can be specified.
The Beavers-Joseph condition is not defined in the case of an unsaturated porous medium. Since the velocity field of the air phase cannot be visualized, both the velocity and velocity gradient at the interface cannot be obtained. The air flow velocity cannot be determined from confocal microscopy, because the flow velocity is too large to allow particle tracking.

4.2.2.1 Velocity field

For a Reynolds number of 871, the air does not invade the porous medium. At the air-water interface, water is dragged along due to the shear stress from the flowing air. This leads to the formations of eddies along the interface. The influence of the eddies is only one pore from the interface. There is a small flow of water in the opposite direction of the air flow. There is no flow of water further inside the porous medium. The air drags along the water at the interface, creating eddies with high flow velocities (around 450 μm/s). The flow pattern is schematically shown in Figure 19. At one pore away from the interface, a flow occurs in horizontal direction, in the direction of the air flow. The velocity is around 30 μm/s, which is very small compared to the air flow rate (Figure 20). At further distances from the interface, no flow occurs within the porous medium.
At high air flow rates, water will drain from the porous medium. At flow rates of 1.0 L/min, where the flow becomes turbulent, drainage occurs immediately. This can occur due to the highly variable pressure field in turbulent flows. This cannot be tested, as the pressure cannot be measured in the experiments in this study.

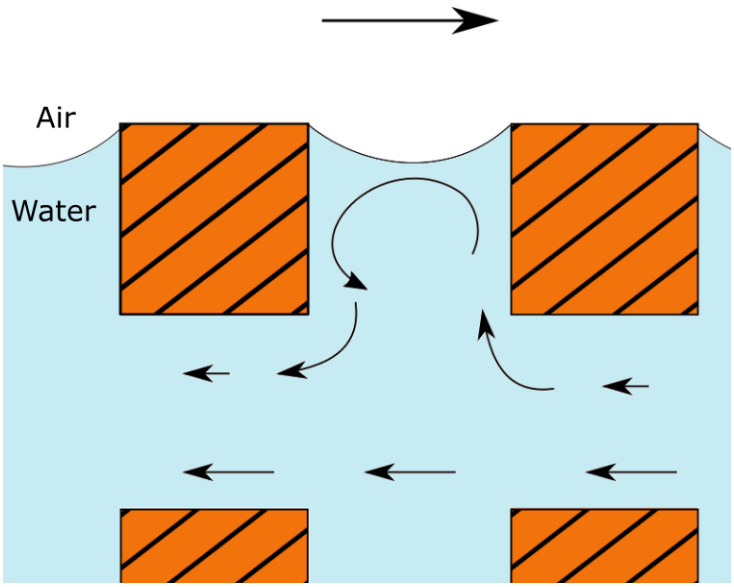

Figure 19: Schematic representation of eddies near the air-water interface.

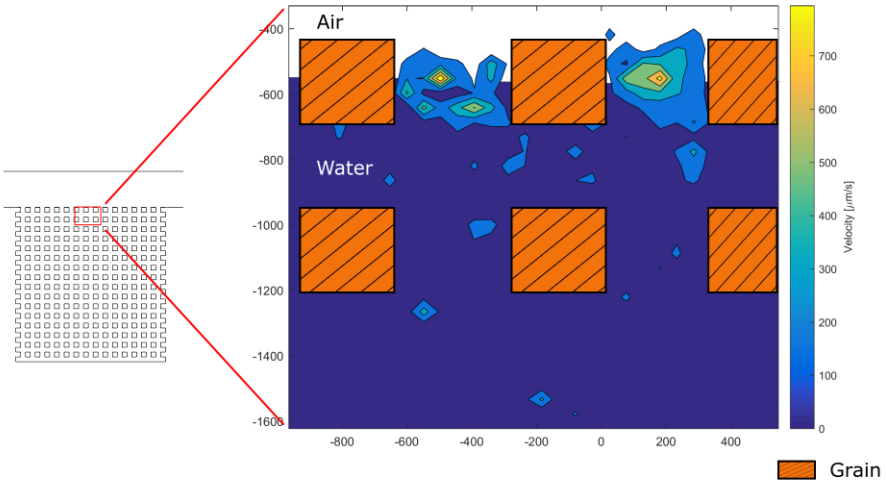

Figure 20: Velocity field and direction for the two-phase experiment. $Q_{air} = 0.4$ L/min.

4.3 Comparison between model and experiments

It has been attempted to simulate the experimental setup in the model. However, some difficulties have been encountered. The pore body and throat radii are set to 125 μm. These pore throat sizes are relatively large for porous media, e.g. mean values in sandstone are 50 μm (Lindquist et al., 2000). Also, the throat radius is equal to the body radius. Therefore, the assumption that the pore throat is the restricting factor is invalid. Pore bodies do also have a resistance to flow. Omitting this resistance would likely lead to an overestimation of the pore velocity. To the author's knowledge, there are no pore-network models that include a conductivity for pore bodies described in the literature. Another consequence of the large pore throats is that the entry pressure of the pore throats is relatively small (1086 Pa, for the parameters given in Table 2). Because of the small pressure required for invasion of the network, the saturation of the pore body is still high when neighboring throats are invaded. Thus, non-wetting fluid will invade the network while it is still mostly saturated. The saturation will stop changing once the non-wetting phase reaches the wetting reservoir.
An important problem is that the Stokes model does not converge when large velocities are set as a boundary condition at the interface. Large flow velocities occur due to the combination of large

throat radii and small throat lengths. The flow rates increase when using less viscous fluids. The pore throat velocity is larger for fluids with a low viscosity. In this study, the Stokes model uses the box-method (Huber and Helmig, 2000), which might not be the most ideal method for solving the Stokes equations. This method might lead to pressure oscillations, which might contribute to the models instability. A staggered grid approach will remove the pressure oscillations and might make the model more stable (Samantray, 2014). Alternatively, the flow velocities might be too large for the Stokes equation, and the Navier-Stokes equation should used in these situations.
In the case of two-phase flow, invasion of the network by the non-wetting phase is determined by the non-wetting pressure at the inlet pores. However, the pressure in the micromodel cannot be measured. Since pressure is the parameter that determines invasion of the model, it would be valuable to be able to measure the pressure in the micromodel.
Experiments show that eddies form in the water near the interface due to the drag force of the air. This leads to a small flow of water in the direction of the air flow. However, the porous medium is not invaded. In the pore-network model, it is not possible to model this situation. If the pore-network is not invaded, water will not flow. Once invasion occurs, water in the network will drain towards the outlet. There is some flow in horizontal direction, in the direction of flow in the freeflow domain, due to the pressure gradient at the interface. However, this flow is several orders of magnitude smaller than the vertical flow. Water drains towards the outlet because the pressure at the outlet is set to zero. If a value larger than zero is assigned to the outlet, drainage and imbibition will alternate each timestep. For one timestep, water will drain from the pore-network and moves towards the outlet pores. The next timestep, water will flow from the bottom of the pore-network towards the top. However, water will not enter the Stokes domain, since the wetting-phase throat conductivity is set to zero for the inlet throats. Becausing of the alternating drainage and imbibition regimes, the saturation in the network will remain almost constant. There is no lateral flow in this case.

This study shows that it is feasible to include pore scale effects in coupled freeflow and porous medium systems. However, the experimental setup could not be recreated perfectly in the model. The pore throats have too large radii and too short lengths. Therefore, the flow at the interface is relatively large, and the Stokes model cannot converge. However, in the case of single-phase flow, the flow pattern can be modeled accurately. Similar velocities could not be obtained, because a smaller pore throat size has to be used in order for the model to converge. Therefore, the model underestimates the velocity in the pores.

5 Conclusions

At the interface between a porous medium and freeflow domain, a transition of flow properties occurs. A complex interface is required for adequate description of the transfer processes that occur there. In previous research, a pore-network model was suggested as a possible method of describing the interface. The aim of this study was to take the first step and couple a freeflow model to a pore-network model, in order to describe the pore-scale processes at the interface. Both single-phase and two-phase flow have been considered. In the two-phase model, the freeflow domain is occupied by the non-wetting phase. A dynamic pore-network model is used for the two-phase situation. In the freeflow domain, the Stokes model is solved. Additionally, the freeflow-porous medium interface was investigated experimentally using confocal microscopy. A micromodel has been built, containing a freeflow domain and a porous medium. The velocity field was determined using particle tracking.

The model is able to describe mass transfer between the pore-network and the freeflow domain accurately. The velocity field in both the simulations and experiments show similar patterns. However, care must be taken that the velocity at the interface in the freeflow region is not too large, otherwise the Stokes model has trouble converging. Large flow velocities occur due to large pore throat radii and small pore throat lengths. The pores in the micromodel are too large and cannot be used in the simulations, as the Stokes model cannot converge due to the large velocities at the interface. At the interface between the pore-network and freeflow domain, continuity of mass flux and normal stress are used as coupling conditions. For the tangential velocity in the freeflow domain, the Beavers-Joseph condition was used. The continuity of normal stress condition leads to a pressure jump at the interface, due to the different model concepts. The magnitude of the pressure jump was investigated and was determined to be negligibly small. The model was run with both the continuity of normal stress and continuity of pressure, but the results were the same. In the case of two-phase flow, the model is able to model drainage at low flow velocities in the freeflow domain. Experiments show that a water flow occurs due to the drag force of the air. However, air does not invade the porous medium. This cannot be recreated in the pore-network model, as water flows only once the network is invaded. However, drainage of the pore-network can be modelled accurately.

This work shows the potential of including pore-scale processes at the interface in coupled freeflow and porous media systems, as mass transfer between the freeflow domain and pore-network can be successfully described for both single-phase and two-phase flow situations. However, this study also highlights difficulties which have to be tackled in further research. The most important one is that the Stokes model used in this study has trouble converging. The use of the Navier-Stokes equation instead of the Stokes equation might resolve the issues that occur at large flow velocities. Otherwise, a more stable method of solving the Stokes equations can be investigated. The model can be extended to include component and heat transport. Then, processes like evaporation can be modelled, which might be an important process when invasion of the network does not occur. The pore-network model is used as a description of the thin layer between the freeflow domain and the porous medium. This is a transition zone of the material and fluid properties. Therefore, a macroscopic model of a porous medium will be attached to the bottom of the pore-network model. Here, Darcy's law, modified for two-phase flow, will be solved. Some changes have to be made to the dynamic pore-network model. In this study, no air is allowed to pass through the pore throats at the outlet. This has to be altered, as the non-wetting phase must be able to flow towards the two-phase macroscopic porous medium. Additional boundary conditions are required if the pore-network is also coupled to a Darcy-scale porous medium at the outlet. Since the pressure at the inlet is the most important parameter controlling flow in both single- and two-phase situations, it would be valuable to be able to measure the fluid pressure in the micromodel.

References

R.C. Acharya, S. E. van der Zee, and A. Leijnse. Porosity-permeability properties generated with a new 2- parameter 3d hydraulic pore-network model for consolidated and unconsolidated porous media. *Advances in Water Resources*, 27:707–723, 2004.

M. I. S. Azzam and F. A. L. Dullien. Flow in tubes with periodic step changes in diameter: a numerical solution. *Chemical Engineering Science*, 32:1445–1455, 1977.

K. Baber. *Coupling free flow and flow in porous media in biological and technical applications: From a simple to a complex interface description.* PhD thesis, University of Stuttgart, Stuttgart, Germany, 2014.

G. S. Beavers and D. D. Joseph. Boundary conditions at a naturally permeable wall. *Journal of Fluid Mechanics*, 30:197–207, 1967.

M. J. Blunt. Flow in porous media - pore-network models and multiphase flow. *Current Opinion in Colloid and Interface Science*, 6:197–207, 2001.

H. C. Brinkman. A calculation of the viscous force exerted by a flowing fluid on a dense swarm of particles. *Appl. Sci. Res.*, A1:27–34, 1947.

D. B. Das and M. Lewis. Dynamics of fluid circulation in coupled free and heterogeneous porous domains. *Chemical Engineering Science*, 62:3549–3573, 2007.

M. Discacciati and A. Quarteroni. Navier-stokes/darcy coupling: Modeling, analysis, and numerical approximation. *Rev. Mat. Complut.*, 22:315–426, 2009.

M. Ehrhardt. An introduction to fluid-porous interface coupling. *Progress in Computational Physics (PiCP). Coupled Fluid Flow in Energy,j Biology and Environmental Research*, pages 3–12, 2010.

B. Flemisch, M. Darcis, K. Erbertseder, B. Faigle, A. Lauser, K. Mosthaf, S. Müthing, P. Nuske, A. Tatomir, M. Wolff, and R. Helmig. Dumux: Dune for multi-Phase, Component, Scale, Physics, ... flow and transport in porous media. *Advances in Water Resources*, 34:1102–1112, 2011.

B. Goyeau, D. Lhuillier, D. Gobin, and M. G. Velarde. Momentum transport at a fluid-porous interface. *International Journal of Heat and Mass Transfer*, 46:4071–4081, 2003.

S. M. Hassanizadeh and W. G. Gray. Derivation of conditions describing transport across zones of reduced dynamics withing multiphase systems. *Water Resources Research*, 25:529–539, 1989.

R. Huber and R. Helmig. Node-centered finite volume discretizations for the numerical simulation of multiphase flow in heterogeneous porous media. *Computational Geosciences*, 4:141–164, 2000.

V. A. Jambhekar, R. Helmig, N. Schröder, and N. Shokri. Free-flow-porous-media coupling for evaporation-driven transport and precipitation of salt in soil. *Transport in Porous Media*, 110: 251–280, 2015.

V. Joekar-Niasar. *The immiscibles: capillarity effects in porous media.* PhD thesis, Utrecht University, Utrecht, The Netherlands, 2010.

V. Joekar-Niasar, S. M. Hassanizadeh, and H. K. Dahle. Non-equilibrium effects in capillarity and interfacial area in two-phase flow: dynamic pore-network modelling. *Journal of Fluid Mechanics*, 655:38–71, 2010.

W. J. Layton, F. Schieweck, and I. Yotov. Coupling fluid flow with porous media flow. *SIAM Journal of Numerical Analysis*, 40:2195–2218, 2003.

W. B. Lindquist, A. Venkatarangan, J. Dunsmuir, and T. F. Wong. Pore and throat size distributions measured from synchotron x-ray tomographic images of fontainebleau sandstones. *Journal of Geophysical Research*, 105:21509–21527, 2000.

K. Mosthaf, K. Baber, B. Flemisch, R. Helmig, A. Leijnse, I. Rybak, and B. Wohlmuth. A coupling concept for two-phase compositional porous-medium and single-phase compositional free flow. *Water Resources Research*, 47:W10522, 2011.

J. A. Ochoa-Tapia and S. Whitaker. Momentum transfer at the boundary between a porous medium and a homogeneous fluid - i. theoretical development. *Journal of Heat and Mass Transfer*, 38: 2635–2646, 1995.

T. C. Ransohof and C. J. Radke. Laminar flow of a wetting liquid along the corners of a predominantly gas-occupied noncircular pore. *Journal of Colloid and Interface Science*, 121:392–401, 1988.

A. Raoof, H. M. Nick, S. M. Hassanizadeh, and C. J. Spiers. Poreflow: A complex pore-network model for simulation of reactive transport in variably saturated porous media. *Computers and Geosciences*, 61:160–174, 2013.

P. G. Saffman. On the boundary condition at the surface of a porous medium. *Studies in Applied Mathematics*, 50:93–101, 1971.

P. Samantray. Implementation of advanced algebraic turbulence models on a staggered grid. Master's thesis, University of Stuttgart, Stuttgart, Germany, 2014.

N. Schwenck, M. Beck, B. Becker, H. Class, T. Fetzer, B. Flemisch, C. Grüninger, J. Hommel, V. Jambhekar, A. Kissinger, T. Koch, M. Schneider, N. Schröder, G. Seitz, and K. Weishaupt. Dumux 2.8.0. 2015. doi:10.5281/zenodo.31611.

K. E. Thompson. Pore-scale modeling of fluid transport in disordered fibrous materials. *AIChE Journal*, 48:1369–1389, 2002.

A. M. Vidales, J. L. Riccardo, and G. Zgrablich. Pore-level modelling of wetting on correlated porous media. *J. Phys. D: Appl. Phys.*, 31:2861–2868, 1998.

E. W. Washburn. The dynamics of capillary flow. *Physical Review*, 17:273–283, 1921.

D. Zhou, M. Blunt, and F. M. Orr. Hydrocarbon drainage along corners of noncircular capillaries. *Journal of Colloid and Interface Science*, 187:11–21, 1997.